Ocean Engineering 244 (2022) 110297

Contents lists available at ScienceDirect

Ocean Engineering

journal homepage: www.elsevier.com/locate/oceaneng

Simplified test program for hydrodynamic CFD simulations of wind-powered cargo ships

Jarle Vinje Kramer *, Sverre Steen

Department of Marine Technology, Norwegian University of Science and Technology, Otto Nielsens veg 10, 7052 Trondheim, Norway

ARTICLE INFO

Keywords:
Computational Fluid Dynamics
Wind-power
Hydrodynamics
Simplifications
Rudder model

ABSTRACT

Four practical simplifications for modeling the hydrodynamic properties of a wind-powered cargo ship with CFD and a route simulation model is evaluated. We first test how much the drift-induced hull forces are dependent on Froude number, model scale, and heel angle. Then, we test the mathematical assumptions in the MMG maneuvering model, with particular focus on the rudder resistance as a function of drift angle, rudder angle and propeller thrust. The overall goal is to see if the hydrodynamics of the ship can be modeled with both a simplified CFD setup and a simplified route simulation model. For each tested simplification, we find that they can be used under specific conditions, but not always. We give specific recommendations based on our results. To improve the predicted rudder resistance from the MMG model, we suggest a slightly modified model based on classical lifting line theory. All the numerical experiments are performed using the open source CFD library OpenFOAM. The simulation setup is described, including details of the mesh design. The numerical uncertainty is quantified, and the simulations are compared against benchmark experiments.

1. Introduction

Modern sail technology, such as wing-sails, rotor sails, and kites, can significantly reduce a cargo ship's fuel consumption. Some examples of the benefit of wind power are shown in Ouchi et al. (2013), Tillig et al. (2020), Kramer et al. (2016a), and Väinämö (2017) where the estimated reduction in fuel consumption is between 8%–48%. However, the wind generated thrust is not without its challenges. For practical cargo ship velocities and wind conditions, there is usually a side force from the sails that is several times larger than the thrust (Kramer et al., 2016a). The aerodynamic side force and the resulting yaw moment must therefore be balanced by opposite hydrodynamic forces. Depending on the longitudinal placement of the sails, this is achieved by generating a lift force on both the hull and the rudder by moving with a steady drift and rudder angle. Additionally, the sails will often apply a significant heel moment, as the side force is effectively acting at a position far above the deck. When the hull rotates to balance the heel moment, the hydrodynamic properties of the ship might change. These hydrodynamic effects are important to consider for a wind powered vessel as they can significantly increase the calm water resistance. The fuel savings due to wind-power might be overestimated if the effect of the side force is neglected and the side force can have an influence on how the sails should be operated (Kramer et al., 2016a).

To quantify the benefit of wind-power for a given ship design, it is common to perform route simulations where a model of the ship and the sails are used together with weather data. The hydrodynamic model of the ship mus be able to calculate the resistance, side force, yaw moment and heel moment as a function of the aerodynamic forces if the added resistance due to the sails is included in the simulation. Although there is no standard way of modeling these things, it is common to use models from ship maneuvering theory, either directly or as inspiration. Two examples of this type of modeling can be found in Tillig et al. (2020) and Kramer et al. (2016a).

Depending on the mathematical form of the hydrodynamic model used in the route simulation, there are usually several design specific coefficients that needs to be estimated based on some method. In the earliest stages of a design phase, purely theoretical or empirical methods might be a good choice (Tillig, 2020; Tillig et al., 2020; Tillig and Ringsberg, 2020). At the end of the design phase, the ship can be thoroughly tested with either Computational Fluid Dynamics (CFD), towing tank experiments, or both. The data from experiments or simulations are then used to tune the coefficients in the model so that the forces and moments predicted by these models are as close to the tuning data as possible. CFD is also a potential tool for the middle of the design phase, where several different geometries of both the hull and the rudder need to be tested. However, during an iterative design loop, long simulation times quickly becomes impractical. To generate a complete hydrodynamic model of the ship, several variables must

* Corresponding author.
E-mail address: jarle.a.kramer@ntnu.no (J.V. Kramer).

https://doi.org/10.1016/j.oceaneng.2021.110297
Received 4 February 2021; Received in revised form 12 November 2021; Accepted 28 November 2021
Available online 21 December 2021

be accounted for and the required number of tests can easily become high. A quick and simplified approach is therefore beneficial, but it is also important to be aware of potential inaccuracies introduced by a simplified approach.

This paper explores four practical simplifications that can be used when generating a hydrodynamic route simulation model of a wind powered ship based on CFD results. We focused on simplifications that are already used in the scientific field, but where we believe there is a need for better documentation of the accuracy. The tested simplifications are listed below, with further explanation in the following paragraphs:

- Neglect the free surface for the computation of drift-induced forces.
- Compute drift-induced forces in model scale
- Neglect the effect of heel on the drift-induced forces
- Use an established maneuvering model – the MMG model – as basis for a route simulation model

All of these simplifications reduce the complexity and time for setting up a hydrodynamic model of a wind powered ship, but they also introduce potential errors in the estimated forces and moments. The main question in this paper is: how large is the error introduced by each simplification? We explore this question by using a case study of a 5000 DWT general cargo ship. The magnitude of the error is discussed in regards to predicting the hydrodynamic resistance of wind-powered ships under the influence of a side force from sails. We focus exclusively on the hydrodynamics, and the aerodynamics of the sails and other aspects of route simulations are therefore not addressed directly.

Neglecting the free surface allows for a considerable speed up of a CFD simulation due to several factors: the physical model becomes simpler without the free surface dynamics, the mesh size can be reduced when the geometry above the free surface is not part of the simulation, and it may allow for time-efficient steady-state solvers. Although it is well-known that the wave resistance of a ship is significant for practical cargo ship Froude numbers, it is less clear how maneuvering coefficients and drift-induced forces are affected by the free surface. It is common to neglect the free surface in maneuvering simulations when the Froude number is lower than approximately 0.15 (Ohashi et al., 2018) while the free surface is usually included for higher Froude numbers (Duman and Bal, 2019). Although it is natural that the waves generated by the ship will affect the drift-induced forces at some point, the exact limit on the Froude number is unclear in the existing work. We have previously studied drift-induced forces on a low aspect-ratio foil geometry, both experimentally (Kramer et al., 2016b) and with CFD (Kramer and Steen, 2015), and concluded that the free surface effects where small for Froude numbers up to approximately 0.25. Longo and Stern (2002) presents experimental data for the drift-induced forces on the ship geometry Series 60 for a wide range of Froude numbers. The results indicate that the side force and drift-induced drag only differ with up 11% for Froude numbers between 0.1 and 0.3. Due to the computational practicality of neglecting the free surface, we wanted to test this simplifications for our case study ship for Froude numbers between 0.15 and 0.3.

Small scale models are routinely used to test drift-induced forces on ships. This is done both in experiments (van der Kolk et al., 2019) – where the size of the model is limited by the size of the towing tank – and in simulations (van der Kolk et al., 2020) — where reduced model size is used to increase the relative cell size close to solid walls and therefore reduce the total mesh size and computational time. The drift-induced force coefficients are usually not scaled based on Reynolds number. However, there are also papers in the literature that indicate that this is not a very accurate approach for computing full-scale drift-induced forces and maneuvering coefficients. One example is Jin et al. (2016), which shows the result from numerical experiments of both static drift and pure sway for the ship geometry KVLCC2 at model scales 1:58, 1:100, 1:225, and 1:1. The results indicate that the yaw moment is not much affected by scale effects, but the sway force is overpredicted by as much as 21.3% in the static drift test and 27.4% in the pure yaw test. Another example can be found in Bhushan et al. (2009) which shows results from a 20/20 zig-zag test of the ship geometry DTMB 5415 in a model-scale of approximately 1:211 and full-scale. The results show that both the rudder checks and the overshoot on the heading angle is overpredicted in model scale, by 5% and 13% respectively. As such, these papers indicate that too low Reynolds number might be problematic for estimating full-scale drift-induced forces. At the same time, they both focus on model scales suitable for physical towing tanks while CFD simulations are not restricted by physical limitations. We therefore wanted to test how the drift-induced forces on a ship depend on the Reynolds number, and whether there exists a scale large enough to avoid scaling issues on the drift-induced force coefficients, yet small enough to speed up the CFD simulations considerably relative to full-scale simulations.

Neglecting heel when computing the drift-induced forces on a ship is practical as it removes an entire state variable from the model, and therefore the number of necessary CFD simulations. It is also a simplification that is common in existing maneuvering models (Yasukawa and Yoshimura, 2015; Abkowitz, 1964), even though a maneuvering ship can experience significant heel angles. For instance, Bhushan et al. (2009) show an example of a ship that experiences heel angles in the range of −18 degrees to +15 degrees during a standard 20/20 zig-zag test. Bertram (2000) states that the effect of heel on drift-induced forces is small for many practical maneuvering situations for cargo ships, but that it must be included for situations where the heel angle exceeds 25 degrees. This limit is well above what we expect will be the case for wind-powered merchant ships. Although the experienced heel angle might be large for conventional sailing vessels, such as regatta boats and pleasure crafts, there will probably be strict limits for wind-powered cargo ships that must be enforced by the control system of the sails. The recommended limit on the heel angle due to steady continuous wind loads is for instance 16 degrees in the DNV stability classification rules (DNV-GL, 2016). This is because continuous operation with large heel angles could be problematic for cargo storage, the comfort of the crew, and generally pose a safety risk. Neglecting the effect of heel on the drift-induced forces therefore seemed like a possible simplification for route simulations of wind-powered ships, but we also saw it as necessary to test this simplification further due to lack of existing validation in the literature.

The final simplification evaluated in this paper is to utilize the simplicity of the MMG model to reduce the number of CFD simulations for a given ship design to a minimum. This is a widely used maneuvering model that contains several practical simplifications for modeling the forces on a ship as a function of drift angle, yaw rate, rudder angle and propeller thrust. In particular, the interaction between the rudder, hull and propeller is treated with models containing relatively few variables. If the assumptions in the model are appropriate, the model can be tuned using the results from just a few CFD simulations, while still be accurate for state values not directly tested. The accuracy of several of the assumptions in the model regarding hull forces and rudder sway force has been tested before (Yasukawa and Yoshimura, 2015). Although not directly related to the MMG model, similar simplifications on the rudder forces are also explored in Molland and Turnock (1995, 2002) with good results. However, we have not seen any examples in the scientific literature that focus on the model's ability to predict rudder resistance. This might be because this force component is often not that important for maneuvering applications. It is, however, one of the most important variables for route simulations of wind-powered ships. We therefore test all aspects of this model relevant for wind-powered ships, and in particular the rudder resistance at varying propeller loading. We test both the standard version of the MMG model and a slightly modified version where the default rudder model is switched to a classical lifting line model. The reason for this switch was that

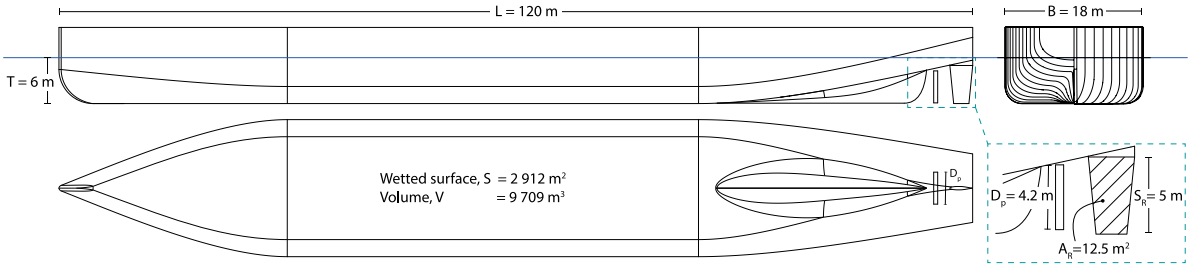

Fig. 1. Illustration of the case study ship geometry.

Table 1
Solver parameters.

	Free surface	No free surface
OpenFoam solver	InterFoam	SimpleFoam
Simulation time	$7L/U$	6000 iterations
Max time step, physical	$0.01L/U$	
Max Courant number	40	
Max alpha Courant number	10	

the default model was found to not be very accurate for the rudder resistance, as will be shown later in this paper.

Section 2 introduces our case study ship along with an overview of the test program for the experiments performed for this paper. The setup of the CFD simulations, along with details of the mesh design is described in Section 3. Section 4 explains the tested route simulation model, including our modifications to the MMG model and the tuning procedure for adjusting the coefficients in the model based on CFD results. Section 5 shows results from convergence studies and validation experiments. Section 6 presents results from the numerical experiments for each simplification along with discussions. We end with our conclusion in Section 7.

2. Case study details

2.1. Ship geometry

The ship tested in this paper represents a 5000 DWT general cargo ship intended to operate at a design speed of 10 knots. The hull shape is a custom geometry with a flat bottom, no bulb, and a slender skeg. An overview of the design with main dimensions, can be seen in Fig. 1. The geometry is also available online at Kramer (2021). The propeller model used in this case study consist of an actuator disk which applies a constant thrust and torque independent of the inflow at the location of the propeller. The rudder is a spade rudder geometry with a taper ratio of 2/3. The foil profile is of the type NASA LS0013, where the thickness is increased from the original 13% to 15%.

2.2. Test performed for this case study

The hull without the rudder is first tested at varying drift and heel angles, at different model scales and Froude numbers. The drift angle is varied between 0 and 12 degrees, while the heel angle is varied between −20 and +20 degrees. The Froude number is varied between 0.15 and 0.3, which corresponds to full scale speeds of 10, 13.3, 16.7 and 20 knots. The model scale is varied between 1:20 and full scale. Most of the tests in this paper is done at the model scale 1:4, corresponding to a model length of 30 m and Reynolds number of approximately 68 million.

We then test the hull and rudder together at zero heel, without the free surface included in the simulation setup, at varying drift and rudder angles both with and without thrust from the propeller actuator disk. The thrust from the propeller corresponds to thrust coefficients equal to 0.5 and 0.25. The largest thrust coefficient is a rounded value that is approximately the necessary thrust for pushing the ship forward at the design speed without wind power. At 10 knots, the full scale ship resistance was estimated to be 75.1 kN. This is based on the results from the CFD simulations shown in Section 6 and conventional scaling methods for ship resistance. With a rough assumption of 10% thrust deduction, this actually corresponds to a thrust coefficient of 0.44 with the chosen propeller dimensions, but we rounded the value up to 0.5 to account for effects not analyzed in this paper, such as added resistance due to wind and waves. We chose to also test a thrust coefficient of 0.25 as a wind powered ship will operate with variable propeller thrust depending on the thrust from the sails. More details regarding our test program is also given along with each simplification in Section 6.

3. CFD setup

The simulations were all performed with the open-source CFD software OpenFOAM v2006+ (OpenCFD ltd, 2021). As part of an effort to ensure both consistency and efficiency when setting up CFD simulations, we use a rule-based scripting approach for setting up simulations implemented in an internally developed Python library. We present the settings used for the simulations in this paper, which matches the rules we apply to ship simulations in general. We have also published the OpenFOAM case folders, including the mesh setup and ship geometry files, for a few representative cases at an online repository found in Kramer (2021). The repository also contains all the custom extensions to the OpenFOAM library we use in this paper.

3.1. Solvers

We used two different OpenFOAM solvers called interFoam and simpleFoam. Both are solving the incompressible version of the Navier–Stokes equation. SimpleFoam is a steady-state solver for single phase fluids, while interFoam is an unsteady solver that allow for two different fluids in one simulation through the use of the Volume-of-Fluid (VoF) method (Hirt and Nichols, 1981). InterFoam use a combination of the PISO-algorithm (Issa et al., 1986) and the SIMPLE-algorithm (Patankar and Spalding, 1983) for solving the pressure–velocity coupling. For unsteady ship applications, we use only the PISO algorithm, with two pressure iterations per time step. SimpleFOAM only uses the SIMPLE-algorithm with relaxation factors for stabilizing the solution.

The time step in the unsteady simulation is adjusted based on two criteria; a physical limit based on ship length an velocity and a mesh limit based on the measured Courant number in the simulations. The physical limit is taken from the ITTC recommendations for practical CFD simulations of ships (International Towing Tank Conference, 2011). The Courant number limit adjusts the time step based on both the flow velocity and the velocity of the Volume of Fluid fraction. The latter is known as the alpha Courant number in OpenFOAM nomenclature. Parameters for the simulation time and time step can be seen in Table 1. In the equations listed, L refers to the ship length and U is the forward velocity of the ship. A convergence study of the time step can be found in Section 5.3.

3.2. Numerical schemes

For the most part we used a fairly standard setup for RANS simulations, with linear upwind schemes for the convection of turbulence variables, central difference for most other variables and a Euler scheme for the time integration in the unsteady simulations. A full overview of our scheme setup can be found in Kramer (2021). The only exception is the interpolation scheme used for the convective term in the velocity equations, where we use the LUST scheme rather than the more typical linear upwind scheme. The LUST scheme is a blend between linear upwind and central difference interpolation with a constant blending factor of 0.25 and 0.75 for the different schemes respectively. In our experimental validation simulations, found in Section 5.6, we have performed several of the tests using both the linear upwind scheme and the LUST scheme with the same mesh. In these tests, the LUST scheme provides slightly more accurate values for the lift and lift-induced drag at large drift angles, and comparable accuracy for the straight-ahead resistance.

3.3. Turbulence model

We used the turbulence model k-ω SST based on the implementation from Menter et al. (2003). The equations used to calculate the inlet values for the turbulence model is shown in Fig. 2. The value for the turbulent energy, k, is based on a target turbulent intensity, I, which is set to 1% for all the simulations in this paper. The equation for the turbulent dissipation rate, ω, is the recommended value from Spalart and Rumsey (2007) which discuss different turbulent inlet values for external aerodynamic flows.

van der Kolk et al. (2020) argue that the simplifications introduced by an isotropic turbulence model could limit the accuracy of drift-induced forces on a ship due to the potentially complex flow structures arising from the separation around the hull. They therefore choose to use an Explicit Algebraic Stress Model (EASM) for their simulations. They also show results for one validation case where the error in the predicted side force with the k-ω SST model is 11.3% while the error with the EASM model is reduced to 4.7%. Although the results presented for the EASM model in van der Kolk et al. (2020) is interesting, OpenFOAM currently has a very limited selection of Reynolds Stress Models, none of which are explicit models. DES and LES alternatives are available, but both options increase the simulation time significantly due to requirements for small time steps. Our choice of the k-ω SST model was motivated by the fact that we get a relatively good match between simulation and experiment for our benchmark experiments using the k-ω SST model (see Section 5.6 for results on this) combined with a lack of good time-efficient alternatives in our chosen simulation software.

3.4. Boundary conditions and simulation domain

The boundaries of the computational domain consist of an inlet, outlet, a top boundary and the boundaries representing the ship geometry. An overview of the computational domain, with boundary conditions, dimensions, coordinate system and locations of the different boundaries can be seen in Fig. 2. The variables listed in the figure refer to the fields included in the simulation. U and p is the velocity and pressure, k and ω is the turbulent kinetic energy and the specific rate of dissipation, and α is the volume fraction of the water. The boundaries of the hull and rudder geometry are specified as no-slip walls with continuous wall functions. When the free surface is not modeled directly, we use a symmetry plane as a boundary condition on the top of the domain, referred to as double body simulations.

There are wave damping zones close to the inlet and outlet in the simulations with free surface modeling. These zones contain body force sources that opposes the ship generated waves. We have made a custom version of wave damping for OpenFOAM simulations that are a direct implementation of the methods presented in Perić and Abdel-Maksoud (2016). The implementation can be found along with the rest of the simulation case files in Kramer (2021). The custom code is automatically complied by OpenFOAM at run time when a simulation is executed.

3.5. Propeller model

The propeller is modeled as an actuator disk where both the thrust and the torque is specified as body forces that varies depending on the radial distance from the propeller center. The purpose of this study was not to test a specific propeller but investigate the effect of propellers in general. As such, we chose the generic theoretical distribution known as the Goldstein optimal distribution (Goldstein, 1929). This distribution represents an ideal propeller with an optimal lift distribution according to simplified lifting line theory. The distribution is adjusted for the presence of a propeller hub, that we assume to have a diameter of 20% of the propeller diameter. The expressions for the radially varying axial force, f_x, and the tangential force, f_θ, are shown in Eqs. (1)–(3). In the same equations, r refers to the non-dimensional radial distance, and r_h to the non-dimensional radial propeller hub location. Both are made non-dimensional by dividing the absolute value by the propeller radius, R_p. T refers to the applied thrust and Q to the applied torque. Δ refers to the total volume of the actuator disk and R_h to the radius of the propeller hub:

$$f_x = r^*\sqrt{1-r^*}\left(\frac{105}{8}\frac{T}{\pi\Delta\left(3R_H+4R_p\right)\left(R_p-R_H\right)}\right) \tag{1}$$

$$f_\theta = \frac{r^*\sqrt{1-r^*}}{r^*\left(1-r_h\right)+r_h}\left(\frac{105}{8}\frac{Q}{\pi\Delta R_p\left(3R_H+4R_p\right)\left(R_p-R_H\right)}\right) \tag{2}$$

$$r^* = \frac{r-r_h}{1-r_h} \tag{3}$$

The propeller body forces are applied to all cells within a disk zone in the mesh with the same diameter and location as the propeller. The thickness of the disk is specified to be 25% of the diameter of the propeller. The mesh resolution inside the propeller disk is set to be one level higher than the resolution at the ship hull in general, which is specified in the next section. The OpenFOAM implementation of the actuator disk can be found in Kramer (2021). The relationship between thrust and torque is taken to be the same as for a four bladed Wageningen B-series propeller (Oosterveld and Oossanen, 1975) with pitch ratio of 1.2 and expanded blade area ratio of 0.8. This corresponds to a propeller that operate with advance ratio of 0.92 and 1.04 and efficiency of 69.6% and 71% for the thrust coefficients of 0.5 and 0.25 respectively.

3.6. Mesh

The mesh was made with the software snappyHexMesh (OpenCFD ltd, 2021), which generates primarily hexadra cells with the possibility of wall layers close to solid objects. The mesh resolution is based on two general rules. The first rule specifies the cell length normal to solid walls. The first layer thickness close to a wall is set to have a length corresponding to a target y+ value, which further depends on the friction on the walls. To estimate the frictional forces ahead of each simulation, an empirical friction line is used. We have chosen a friction line that is specifically tuned to the k-ω SST turbulence model, presented in Eça and Hoekstra (2008) and also shown in Section 3.8. The equations for calculating the thickness of the first layer are presented in Table 2, where L is the ship length, U the ship velocity, ν the kinematic viscosity and C_F the estimated frictional coefficient. The table also show the layer expansion which dictates the increase in thickness for each new layer added, and the ratio between the final layer and the cells outside the wall layers. We use the same layer thickness close to the wall for the hull, skeg and rudder as both the skeg and the rudder are placed in the

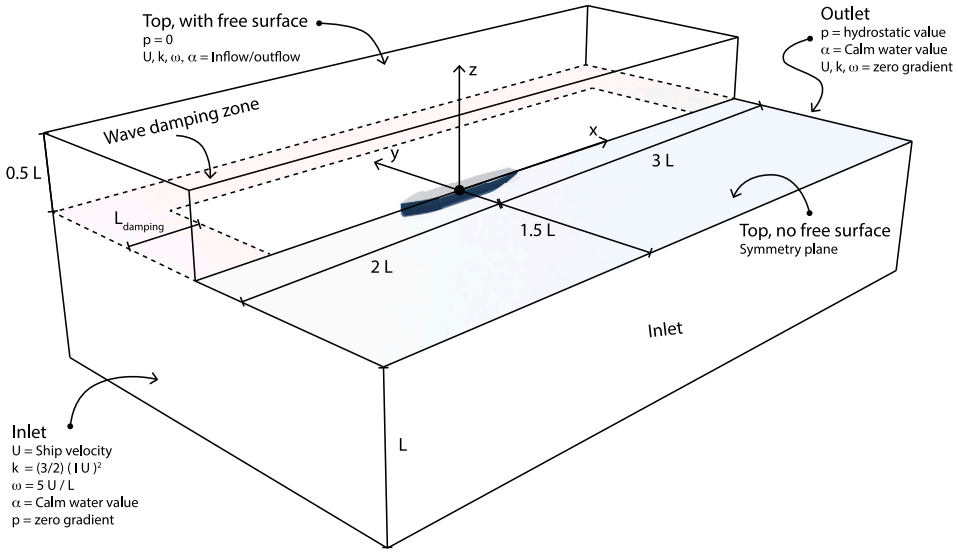

Fig. 2. CFD domain with boundaries and inlet values.

Table 2
Rules for calculating number of wall layers.

Variable	Equation/value
Frictional velocity, u_τ	$\sqrt{0.5C_F U^2}$
Distance to wall center, h_{center}	$y^+_{\text{target}}\nu/u_\tau$
Thickness of first cell, h_{cell}	$2h_{\text{center}}$
Target y + value, y^+_{target}	60
Ratio between last wall layer and first outer cell	0.5
Layer expansion	1.3
Maximum number of layers	15

wake of the ship hull and therefore highly influenced by the boundary layer of the ship. We verified that this assumption was appropriate by checking the achieved y+ values on the different patches for a few representative cases. As an example, for a case with zero drift angle and rudder angle at model scale 1:4, the achieved average y+ value for the hull, skeg and rudder was 67, 75 and 44 respectively.

The second rule changes the resolution in the rest of the mesh based on target cell lengths that are assumed to be independent of the Reynolds number. These target cell lengths are related to patches on the ship geometry and in refinement zones in the wake. Fig. 3 shows the mesh generated for our case study ship from a few different angles at a model scale equal to 1:4. The figure also contains the target cell length at important places relative to the ship length, L. The mesh is shown both for simulations with the free surface present and for simulations without the free surface. The differences are mainly related to refinements areas that are necessary for capturing the ship generated waves and the geometry above the free surface.

To bridge the resolution calculated from the two rules, the number of wall layers are adjusted for each simulation. As we manually fix the wall layer settings, except for the number of layers, it is impossible to always reach a cell length that matches the target cell length in each zone perfectly. As such, we choose the number of layers that most closely match the target cell lengths for each patch. As a result, the actual cell length in the mesh can vary up to 15% in both directions relative to the target cell length when the wall expansion ratio is 1.3. As the mesh resolution outside the wall layers are different on the main hull, skeg and rudder, the number of layers is also different. As an example, for the model scale 1:4, the number of layers on the hull, skeg and rudder is 10, 8 and 3 respectively.

We also limit the number of layers to a maximum as we have experienced problems with the layer generation process in snappyHexMesh when the number of layers gets too high. In these cases, we let the mesh be generated with a higher y+ value than the target value, as this mostly will happen for high Reynolds number flow. The increase in the target y+ values did only occur for model scales larger than 1:4, and the largest target y+ value for the experiments in this paper was 120. We show the effect of different y+ values on a few example cases in 5.4, which indicate that this is an acceptable simplification.

3.7. Forces from simulations

The rudder and the hull geometry is represented as different patches in the mesh, and we can therefore measure the forces on these patches separately. For most of cases without a free surface, the forces appeared completely steady, and we use the value from the last iteration in further post-processing. A few of the cases showed small oscillation on the rudder forces. This indicates a small amount of unsteady behavior, but we then used the average value of the last 1000 iterations as the final value. For simulations with the free surface included, the force on the hull is usually oscillating due to waves bouncing off the boundaries in the simulation domain. Although these waves will die out eventually, due to the wave damping zones, it usually takes an impractically long time. We have found that the mean value of the oscillating signal after the flow has moved 3–5 ship lengths is close to the final mean value when the waves are dampened out.

In order to evaluate the mean value, we fit a harmonic model function with exponentially decaying amplitude to the measured force values by using the values from a time window representing half the simulation length. An example of such a study is shown in Fig. 4. The values from our tuned force model are shown in green, while the dashed green line show the mean value if the model is tuned to every time step in the simulation. The purpose of the latter is to show how the mean value changes over time. We use the same procedure for the side force and the yaw moment, which in general show smaller relative oscillation than the resistance. All force coefficients are made non-dimensional by dividing them by the dynamic pressure, $0.5\rho U^2$, multiplied with a representative area. For the ship hull, the representative area is taken as the length multiplied with the depth, as this is the common area in maneuvering applications. For the rudder, we use the projected rudder area, which are equal to the rudder span multiplied with the mean chord.

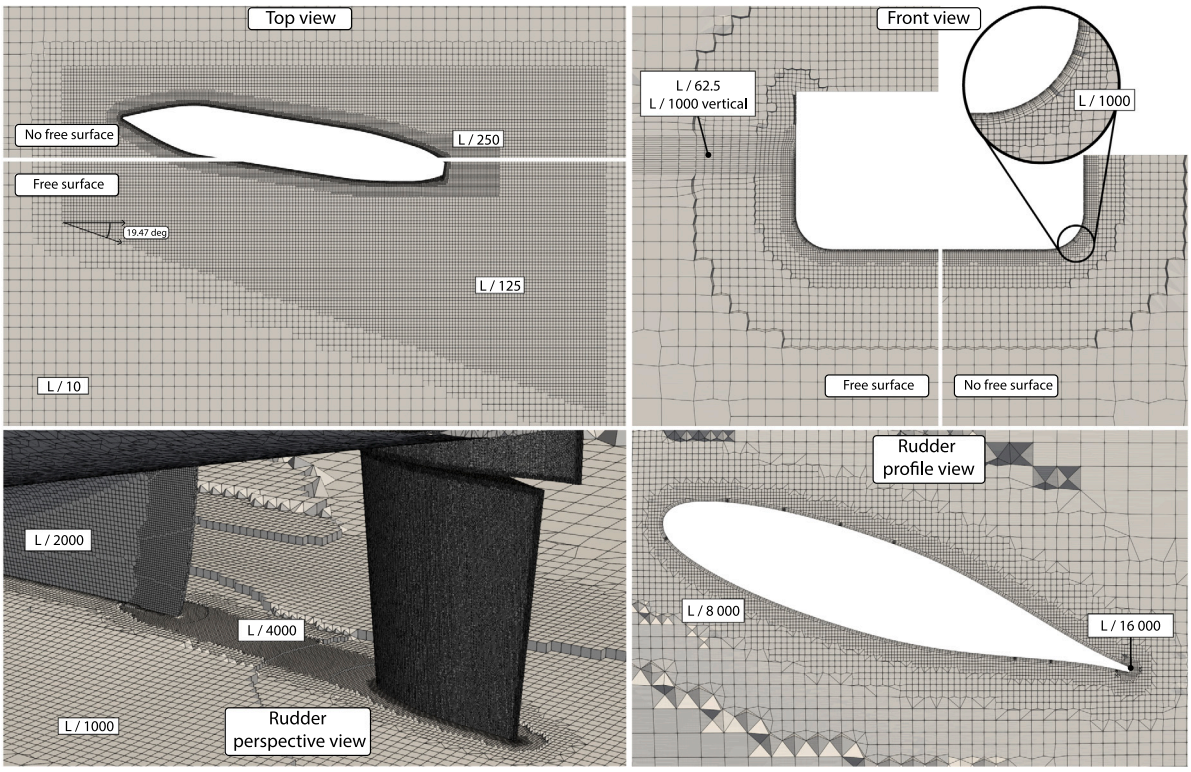

Fig. 3. Mesh illustration.

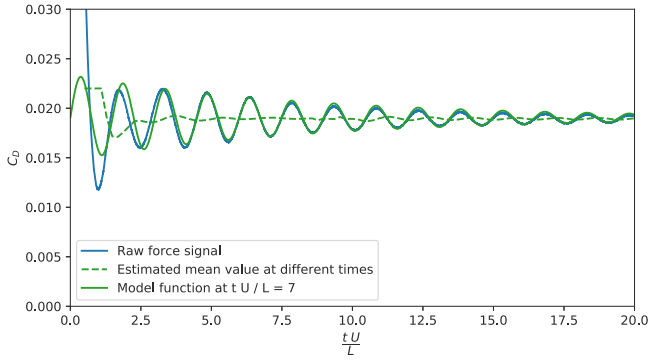

Fig. 4. Post-processing of force signal from simulations with free surface modeling for a case with drift angle equal to 9 degrees. (For interpretation of the references to color in this figure legend, the reader is referred to the web version of this article.)

3.8. Scaling from model scale to full-scale

Only the straight-ahead resistance is adjusted from model scale to full-scale, while drift-induced forces are assumed to be independent of Reynolds number (validity of this assumption is shown in Section 6.2). We assume that the resistance from a simulation without the free surface present can be scaled with a friction line and the wave resistance is calculated as the additional resistance in a simulation with the free surface present. There are many empirical friction lines available, and the most common one in the marine community is the ITT57 friction line. However, as for instance shown in Raven et al. (2008), this default friction line is not always the best choice for scaling ship resistance. As we are scaling results from CFD simulations with the turbulence model k-ω SST, we use a friction line from Eça and Hoekstra (2008), which is tuned based CFD results using the same turbulence model. Equations for this friction line is given below along with the scaling method for the drag coefficient, C_D, from a simulation without the free surface, performed at a Reynolds number Re_0:

$$C_F(Re) = 0.089 Re^{-0.283+4.73\cdot10^{-3}\log Re+2.43\cdot10^{-5}(\log Re)^2} \tag{4}$$

$$C_D(Re) = C_D(Re_0)\frac{C_F(Re)}{C_F(Re_0)} \tag{5}$$

4. Route simulation model

This section presents our current route simulation model, which is a slightly modified version of the MMG model, Yasukawa and Yoshimura (2015). We only show the parts of the model that is relevant for a steady state route simulation of a ship and neglect the terms for modeling inertia forces, added mass effects and forces due to yaw rate of the ship.

4.1. Mathematical formulation

Two different coordinate systems are necessary for this discussion. The MMG model is expressed in a body fixed coordinate system where the x-axis is always aligned with the ships centerline independent of drift angle. However, when discussing the energy consumption of a wind-powered ship, we are mainly interested in the resistance and the side force of the vessel, also known as drag and lift. These forces act parallel and normal to the forward velocity respectively. We call this coordinate system a course fixed coordinate system. An overview of the two different coordinate systems is shown in Fig. 5.

The MMG model is modular and can be divided into three different parts when it is applied as a steady state route simulation model for wind powered ships. The different parts are listed below:

- A model for computing the forces acting on the hull as a function of drift angle and rudder forces
- A model for computing a representative velocity vector for the rudder which includes interaction effects from both the hull and the propeller

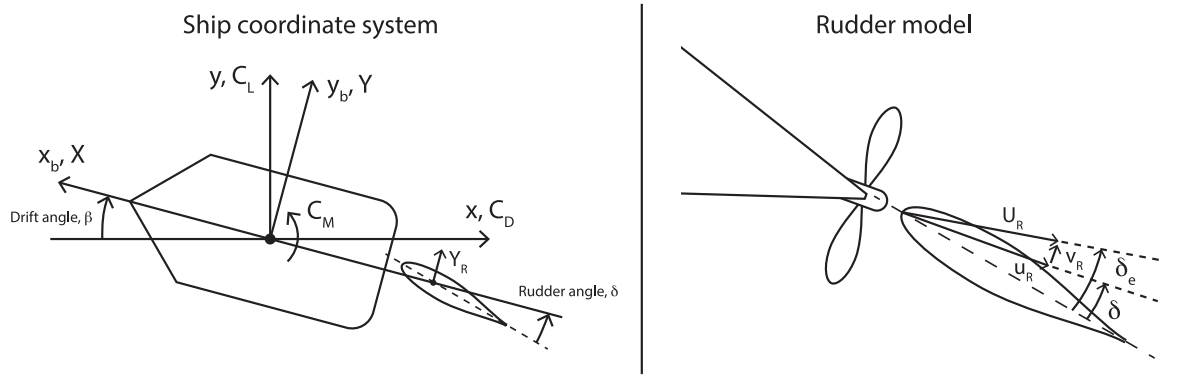

Fig. 5. Coordinate systems used in this paper and an overview of variables in the rudder velocity model.

- A model for computing the forces on the rudder as a function of the single representative velocity vector at the rudder position

The hull surge force, X_H, sway force, Y_H, and yaw moment, N_H, are assumed to be dependent on the sway velocity, v, and the forces on the rudder, X_R, and Y_R. The variable ΔX_R represents the increase in the surge force on the rudder at rudder and drift angles different than zero. The surge force consists of calm water, straight-ahead resistance, R, and otherwise drift- and rudder-induced forces. The model coefficients for the drift-induced forces are given as X_{vv}, X_{vvvv}, Y_v, Y_{vvv}, N_v, and N_{vvv}, while the model coefficients for the rudder-induced forces are given as t_R, a_H and x_H. The complete equations for the hull forces are listed in the equations below:

$$X_H = -R + X_{vv}v^2 + X_{vvvv}v^4 - t_R\Delta X_R \tag{6}$$

$$Y_H = Y_v v + Y_{vvv}v^3 + a_H Y_R \tag{7}$$

$$N_H = N_v v + N_{vvv}v^3 + a_H x_H Y_R \tag{8}$$

The forces on the rudder are assumed to depend on a single representative velocity vector in the body fixed coordinate system represented with the symbols u_R and v_R for the surge and sway velocity. The vector gives both the velocity magnitude and the effective angle of attack on the rudder. The surge velocity is assumed to depend on both the drift angle and the propeller thrust, while the sway velocity is assumed to only depend on the drift angle. The complete model for the rudder velocity vector is listed below:

$$u_R = U(1-w)u_p \tag{9}$$

$$\frac{1-w}{1-w_0} = \left(1 + \left(1 - e^{-C_1|\beta|}\right)\right)\left(C_2 - 1\right) \tag{10}$$

$$u_p = \sqrt{\eta\left(1 + \kappa\left[\sqrt{1+C_T} - 1\right]\right)^2 + (1-\eta)} \tag{11}$$

$$C_T = \frac{T}{0.5\rho A_p U^2} \tag{12}$$

$$v_R = U\gamma\beta \tag{13}$$

$$U_R = \sqrt{u_R^2 + v_R^2} \tag{14}$$

$$\delta_e = \delta + \tan^{-1} v_R/u_R \tag{15}$$

The model contains a single wake factor, w_0, when the drift angle and propeller loading is zero. There are two coefficients that adjust for the effect of drift angle for the surge velocity, C_1 and C_2, while there is just one coefficient, γ, for adjusting the sway velocity. The effect of the propeller thrust is calculated according to classic actuator disk theory. The increase in the surge velocity is dependent on the thrust coefficient of the propeller, C_T, which is calculated as the thrust of the propeller, T, divided by the dynamic pressure multiplied by the propeller disk area, A_p. The variable η is the rudder span divided by the propeller diameter, which adjusts the model for different propeller sizes. There is a single empirical coefficient that needs to be tuned to each case represented by the symbol κ.

The forces on the rudder are calculated based on the representative rudder velocity and a model that represents a general lifting surface. In the standard MMG model, the rudder force is assumed to act normal to the rudder chord for all rudder angles, and the rudder tangential force is completely neglected. The rudder normal force is further assumed to be linearly dependent on the effective rudder angle, which is calculated from the rudder velocity model. The equations for the model are listed below, where f_a is a model coefficient that must be tuned:

$$F_N = 0.5\rho A_R U_R^2 f_a \sin\delta_e \tag{16}$$

$$X_R = -F_N \sin\delta \tag{17}$$

$$Y_R = -F_N \cos\delta \tag{18}$$

$$N_R = -x_R F_N \cos\delta \tag{19}$$

This is a typical model for ship maneuvering applications, but it is also a model that greatly simplifies the relationship between lift and lift-induced drag. For route simulation applications, resistance is an important variable, and we therefore decided to switch to a different rudder model based on classical lifting line theory. However, we kept the rudder velocity model from the standard MMG model. Although this introduce slightly more coefficients to the model, we found this to be necessary in order to accurately model the rudder resistance. A comparison between the original MMG model and the classical lifting line model is shown in Section 6.4.

We assume that the rudder experiences a lift force, L_R, that acts normal to the representative rudder velocity vector and a drag force, D_R, that act parallel to the representative rudder velocity vector. Both the lift and the drag are corrected for the geometrical aspect ratio of the rudder, λ, according to classical lifting line theory, but with empirical correction factors, e_D and e_L, that corrects for the presence of the ship hull, and that can be tuned based on simulation data. The drag model also includes a polynomial for calculating the viscous drag. The equations for our modified rudder model are listed below:

$$C_{L,2D} = 2\pi\delta_e \tag{20}$$

$$C_{L,R} = \frac{C_{L,2D}}{1 + 2/(\lambda e_L)} \tag{21}$$

$$C_{D,R} = a_0 + \frac{C_{L,R}^2}{\pi\lambda e_D} + a_4\delta_e^4 \tag{22}$$

$$L_R = 0.5\rho A_R C_{L,R} U_R^2 \tag{23}$$

$$D_R = 0.5\rho A_R C_{D,R} U_R^2 \tag{24}$$

4.2. Adjusting model coefficients based on CFD results

The coefficients in the model equations are adjusted so that the values predicted by the model is as close to the CFD results as possible. We do this by using a line search optimization algorithm from the SciPy library (Virtanen et al., 2020) to minimize the squared difference between the model predictions and the simulations results, also known as least square regression.

The components in the hull and rudder force model are adjusted separately for each degree of freedom. For instance, the coefficients for the hull surge force are adjusted independently from the coefficients from the hull sway force and the coefficients for the rudder lift is tuned independently from the coefficients for the rudder drag. This is possible as the different models predict the forces in independent directions. For the rudder wake model, the coefficients affects both the rudder lift and drag at the same time. In this case, we minimize the errors from the estimated lift and drag by adding them in the same objective function. We also scale the error measurement so that both values are given approximately equal weight. For this particular case, the rudder lift coefficient is around 10 times larger than the drag coefficient, so the error in the drag is therefore weighted by 10. When we tune the original MMG rudder model, there is only one coefficient that is used to calculate both the lift and the drag at the same time. In this case, we only adjust the model based on the estimated lift. Adding the drag to the tuning procedure could in theory improve the drag accuracy, but not without reducing the lift accuracy. The results from an arbitrary number of CFD simulations can be given to the tuning procedures. We specify which CFD simulations that have been used for the tuning of the models along with the results presented in Section 6.

4.3. Balancing the model

The drift angle and rudder angle in the model can be automatically adjusted to produce a target amount of side force and yaw moment. This functionality is implemented so that the hydrodynamic model can balance externally applied forces and moments from sails. The variables are adjusted with a non-linear numerical solver from the SciPy library, based on the Newton algorithm. There are in total three balancing functions; adjust the rudder angle to reach a target yaw moment, adjust the drift angle to reach a target side force, and a combination function that adjust the drift angle and the rudder angle at the same time. The combination function has two levels. The first level balances the yaw moment for each drift angle, which gives the rudder angle as a function of the drift angle. The second level tunes the drift angle by using the first level. As the rudder angle is adjusted for each drift angle, this balances both the yaw moment and side force at the same time.

5. CFD verification and validation

To estimate the errors and the uncertainty in the simulations we have performed convergence studies and compared our simulation results against experiments. The results from these tests are shown in this section.

5.1. Generalized uncertainty estimate

We follow the general procedure for convergence studies recommended by the ITTC in International Towing Tank Conference (2017), which is to a large degree based on the work presented in Eça et al. (2010). The recommendations presents different methods for estimating the numerical uncertainty based on a parameter convergence test. All methods are based on the concept of Richardson extrapolation (Richardson, 1911). As we use an unstructured mesh, we have chosen to estimate the uncertainty using the least square approach. In this method, the relationship between a simulation value, S_i, at a given parameter value, h_i, and the converged simulation result, S_0, is estimated according to different model functions:

$$S_i = S_0 + ah_i^p \tag{25}$$

$$S_i = S_0 + ah_i^2 \tag{26}$$

$$S_i = S_0 + a_1 h_i + a_2 h_i^2 \tag{27}$$

The coefficients in the equations (S_0, a, p, a_1 and a_2) is found using a least square approach. This requires a set of CFD simulations with different parameter values. A curve fitting algorithm is then used to estimate the coefficients in the equations by minimizing the squared difference between the model prediction and the actual values. We use a line search optimization algorithm from the SciPy library (Virtanen et al., 2020) for this task.

Eq. (25) is first used to make an initial estimate. If the predicted order of accuracy – the value of p – is between 0.5 and 2, the equation is kept as the model function for the parameter variation. If the predicted order of accuracy is larger than 2, the model equation is switched to Eq. (26). If the predicted order of accuracy is less than 0.5, the best fit of Eqs. (26) and (27) is used.

The estimated relative error in the simulation result as a function of the tested parameter is then calculated as $\delta_i = (S_i - S_0)/S_0$. However, there is an exception if the simulation data is seen to oscillate above and below the estimated converged simulation result, S_0. In that case, the simulation error is instead estimated according to the equations below, based on a set of n simulation results with parameter values h_i and simulation results S_i:

$$S_0 = \text{Mean}(S_i) \tag{28}$$

$$\delta = \left(\frac{\text{Max}(S_i) - \text{Min}(S_i)}{h_n/h_1 - 1} \right) / S_0 \tag{29}$$

Finally, the uncertainty, U_i, due to the parameter in question is estimated with a safety factor, F_s, as $U_i = F_s|\delta_i|$. The value of F_s is somewhat ambiguous, but recommended by the ITTC to be 1.25 for situations where there is a good fit between the data and the model equations, and 3.0 for situations where the data is seen to oscillate.

This generalized approach is used both for the mesh convergence and the time step study. At least four different parameter values are used for each Richards extrapolation study. For a more in depth explanation of this method, we recommend either International Towing Tank Conference (2017) or Eça and Hoekstra (2014).

5.2. Mesh convergence

When varying the mesh resolution, we multiply all length factors in the mesh set-up software by the same value so that the cell length at each level in the mesh is changed by the same factor. However, we keep the target y+ value constant for our convergence study and check the y+ dependency in a separate study in Section 5.4. To change the mesh such that the wall layer part remain as constant as possible, we change the mesh with a factor that matches the wall layer expansion ratio. As such, for each variation of the mesh resolution in the convergence studies, the cell lengths in the mesh varies with a factor of 1.3 to some power. This is slightly less than the more typical approach of using the square root of two as a mesh refinement factor but has the benefit that each refinement of the mesh removes exactly one wall layer and replaces it with a finer outer mesh.

The uncertainty related to the grid size for the hull is estimated by performing 5 different mesh convergence studies for different cases. All of them contain the ship hull at a drift angle of 9 degrees. The result of this study can be seen in Figs. 6 and 7. Fig. 6 show the results for the cases with free surface modeling and Fig. 7 show the results without the free surface. We also test the hull and rudder together both with and without the propeller present in the simulation. The drift angle was still 9 degrees, and the rudder angle was 6 degrees. The result of

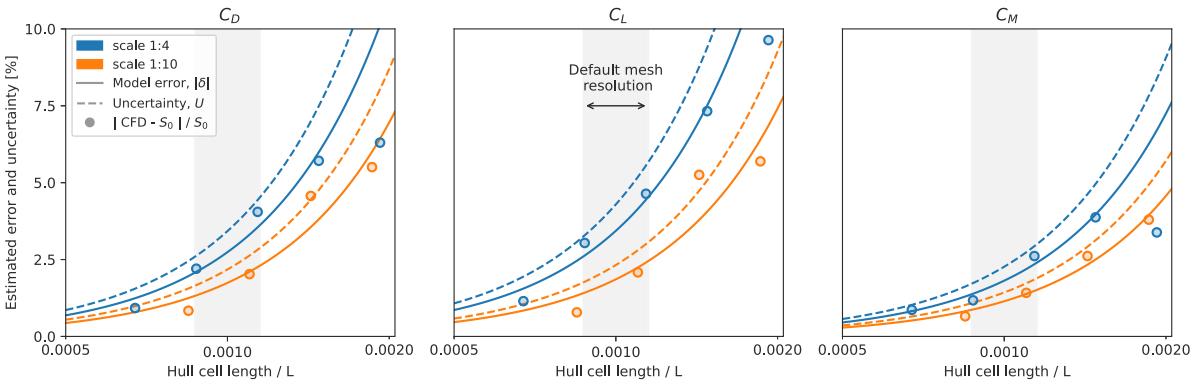

Fig. 6. Convergence study for the hull, without the rudder, with free surface modeling. Drift angle = 9 degrees and Fr = 0.25.

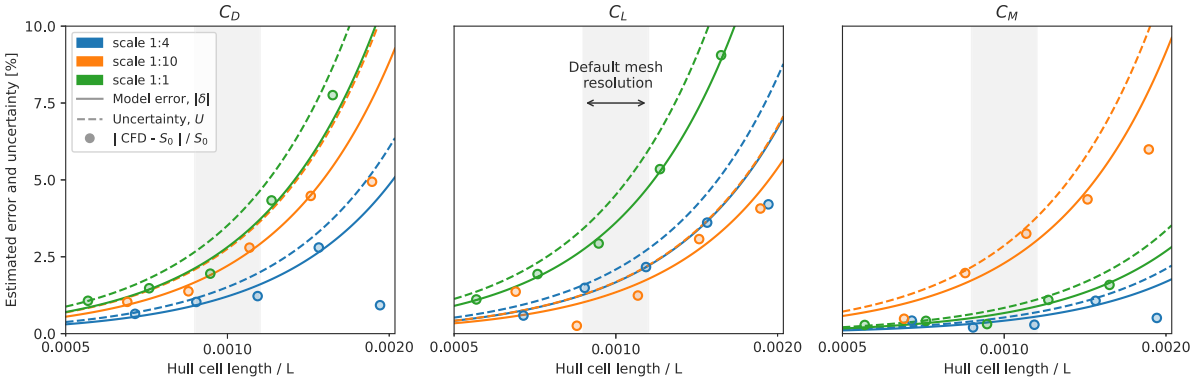

Fig. 7. Convergence study for the hull, without the rudder, without the free surface. Drift angle = 9 degrees.

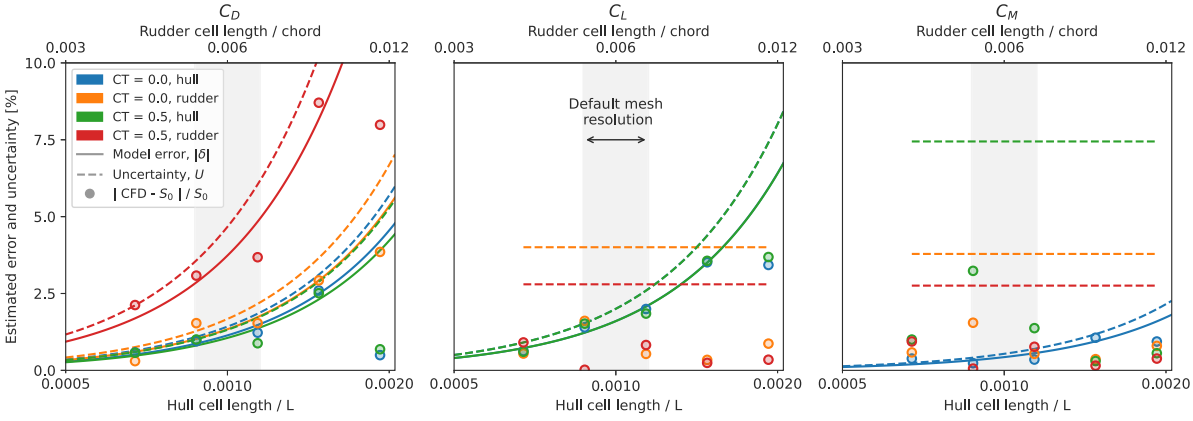

Fig. 8. Convergence study for the hull and rudder together, with and without the propeller actuator disk at a model scale of 1:4. Without the free surface.

this study can be seen in Fig. 8. The plots show the estimated values for the simulation error due to the mesh and the corresponding mesh uncertainty. Both model equation values and CFD values are shown in order to show the fitness of the uncertainty estimate. Most of the cases have an estimated mesh uncertainty well below 5% for the default cell length, and many cases are below 2.5%.

When the estimate for the uncertainty is shown to be a flat line, it is due to oscillating convergence, and the uncertainty is therefore estimated with Eqs. (28) and (29). In these cases, there is a large difference between the CFD values and the estimated uncertainty, due to the large safety factor for oscillating data. However, all of the oscillating cases have result values that are very close together over all the tested mesh resolutions. The largest uncertainty is estimated to be close to 7.5% for the yaw moment on the hull in the case with the hull and rudder together and a thrust coefficient of 0.5. However, the difference between the default cell length and the finest mesh is only 1.7%. We therefore conclude that the mesh resolution is adequate even in the cases where the general Richardson extrapolation has failed to find a good fit of the CFD data.

As mentioned in Section 3.6, the default cell length are allowed to vary within a narrow range to match the outer cell length with the wall layers. The cell length corresponding to our default values (as shown in Fig. 3) is therefore marked with a light gray background that show the range of possible values from our case setup procedure.

5.3. Time step convergence

The effect of changing the time step was tested by simulating the hull alone in the model scale 1:4, Froude number equal to 0.25, and 9 degrees drift angle. Both the physical time step limit and the Courant

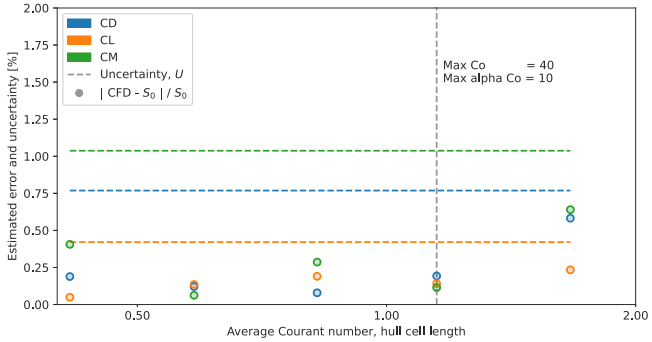

Fig. 9. Time step convergence study, testing a bare hull in model scale 1:4, with free surface modeling, and drift angle equal to 9 degrees.

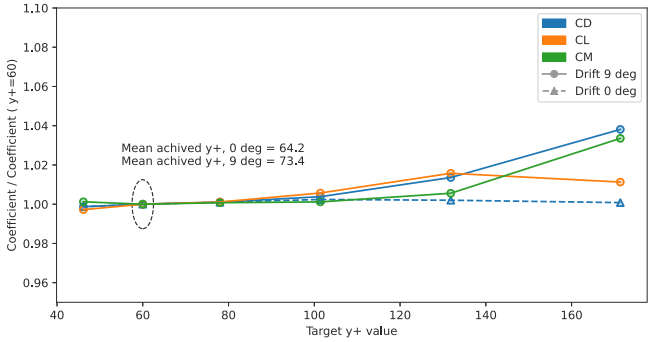

Fig. 10. Effect of target y+ value on the simulated forces at mode scale 1:4.

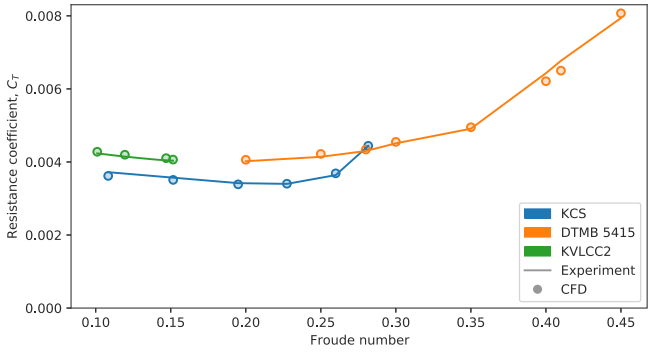

Fig. 11. Calm water straight ahead resistance, from CFD simulations and experiments.

number limits were changed at the same time, although the Courant number limits was the dominating factor in this case. The results from the study can be seen in Fig. 9. The time step change factor was set to the square root of two. The Courant number limits adjust the time step based on the largest measured Courant numbers in the mesh. The time step will therefore vary along with the velocity field over the course of the simulation. In addition, the time step might not change with the same factor as the target Courant number, as the velocity field are altered when the time step is altered. We have therefore plotted the simulated resistance, side force and yaw moment as a function of the average time step in the simulation, made non-dimensional by calculating the average Courant number based on the ship length, ship velocity and the outer cell length at the hull.

Although the convergence study show that the results oscillate over the tested time-steps, the estimated uncertainty is only around 1% or less. This indicate that fairly large maximum Courant numbers are acceptable. However, we have experienced a few cases where the time step must be reduced from the default values due to stability problems with the simulation. This was not a problem for any of the case-study ship simulations in this paper, but it did happen for a few of the validation experiments we show in Sections 5.5 and 5.6. In those cases, we reduced the time step to a maximum Courant number of 20 and maximum interface Courant number of 5.

5.4. Y+ variation

The effect of y+ values was checked separately from the rest of the mesh variation. This was done at the model scale 1:4 for drift angles 0 degrees and 9 degrees, with steady state simulations without the free surface present. The target y+ value was changed by multiplying it with the layer expansion ratio, to different powers. As such, for a change in the target y+ value, only the number of wall layers were changed while all the other mesh parameters where kept constant. The result of this study can be seen in Fig. 10.

Unlike other simulation parameters, it is not necessarily given that a small y+ value provides more accurate results than a large y+ value when wall functions are applied. The achieved y+ values around the hull geometry will vary based on local velocity and friction. Although we use continuous wall functions, the error can still be larger for cells where the local y+ are falling into the transition zone between the logarithmic region and the linear region in the law of the wall. This is for instance shown in Hympendahl and Ciortan (2018), where both continuous and logarithmic wall functions are tested for ship resistance with various simulations codes. Although the continuous wall functions are in general better than purely logarithmic models, the simulation error for both types is shown to increase as the y+ values approach 30. As such, we do not use the generalized Richardson extrapolation model to estimate the uncertainty due to the target y+ value. We do however conclude that the change in force values around our chosen target y+ value of 60 is small, both for larger and smaller values, which suggest that our target value is appropriate. This is also confirmed with the experimental validation in the next two sections.

5.5. Straight ahead resistance

In order to validate our general simulation setup, we have reproduced several experiments published in the scientific literature. For the calm water, straight ahead, resistance, we have chosen the three open ship geometries KCS – a large and fast container ship – KVLCC2 – a large and slow tanker – and DTMB 5415 — a fast naval combatant ship with a sonar dome in the bow. Articles with experimental data and geometry specifications are found the Gothenburg 2010 proceedings, which are summarized in Larsson and Stern (2014). The results from our validation cases are plotted in Fig. 11. The simulation setup for every case is mostly based on the same rules as the one presented for the case study in this paper, including the same mesh resolution. The ship model in the experiments and the simulations where free to move in both heave and pitch. More details of the simulation setup for the validation experiments can be found online in Kramer (2021). The mean error in the predicted resistance from the CFD simulations are 1.21% for all the ship geometries and Froude numbers, while the maximum error is 4.07%. The largest error occurs for the DTMB 5414 at Froude number equal to 0.41.

5.6. Drift-induced forces

In order to validate the drift-induced forces on the hull we used two different validation experiments, with three different ship geometries in total. The first experiment is published in Kramer et al. (2016b), and tests the drift induced forces on different foil shapes, with varying depths at two different Froude numbers. The depths were chosen such that depth to length ratio of the foils where close to typical values for cargo ships, and the geometries were therefore called foil-ships.

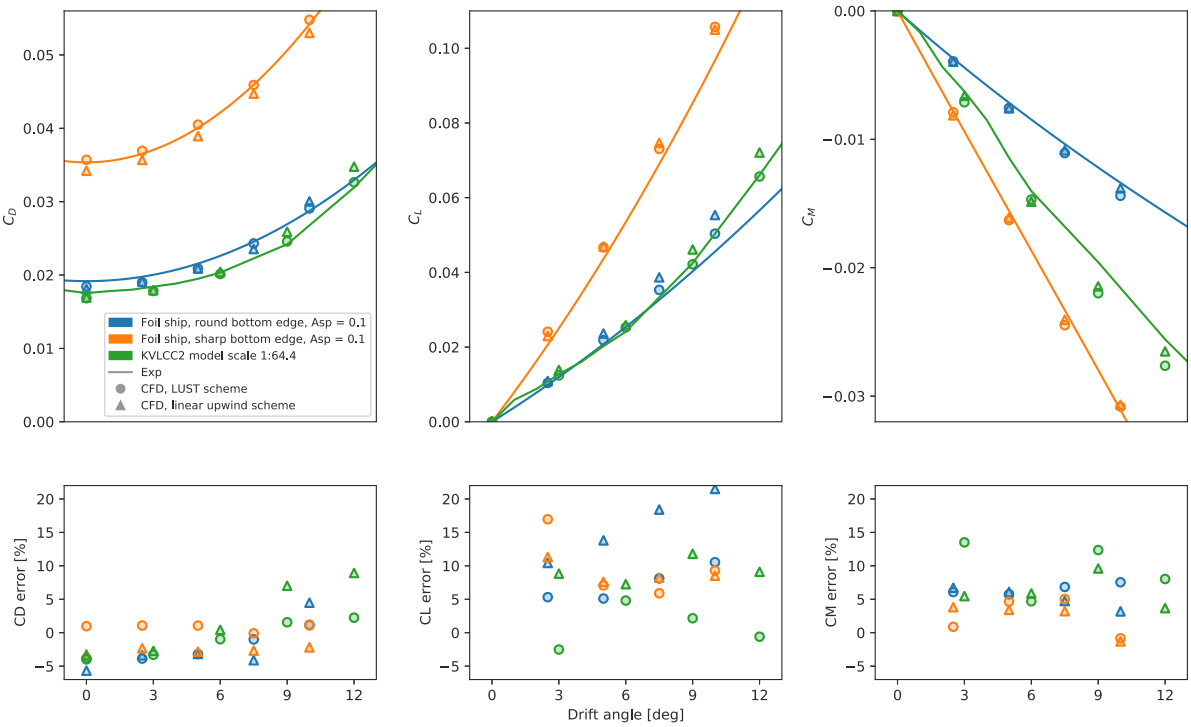

Fig. 12. Experimental validation of drift-induced forces on ship geometries.

For each depth, two different versions of the bottom edge shape were tested; one perfectly sharp and one with a rounded edge. The second experiment can be found in Kume et al. (2006). It consists of experimental data for the forces and moments acting on the tanker ship KVLCC2 at different drift angles at model scale of 1:64.4.

The comparison between experimental data and our CFD data can be seen in Fig. 12 which also show the simulation error defined as the difference between the simulated value and the experimental value, divided by the experimental value. We have performed all the validation experiments with the both the LUST scheme for the convective term, and with the more conventional linear upwind scheme. For large drift angles, the linear upwind simulations tend to overestimate both the lift and the lift-induced drag. This is seen to be less of a problem with the LUST scheme, which is why we have used this scheme for the rest of the simulations in this paper. The tested mesh resolution is the same as for the straight-ahead resistance validation cases described in Section 5.5.

The average absolute value of the error for the LUST scheme is 1.96%, 5.23% and 5.08% for the drag, lift and yaw moment respectively. The same values for the linear upwind scheme are 4.11%, 9.28% and 3.52%. The largest errors are observed for lift at the larger angles of attack. For the round foil ship, the error in the lift is 10.5% with the LUST scheme and 21.5% with the linear upwind scheme. For the KVLCC2 at drift angle equal to 12 degrees, the error is −0.6% with the LUST scheme and 9.1% with the linear upwind scheme. For the sharp foil geometry, the error is comparable with the LUST scheme and the linear upwind. At 10 degrees drift, the error is 10.5% and 9.3% for the LUST scheme and the linear upwind scheme. We suspect this is because the flow separation around the bottom edge is easier to predict with a sharp bottom edge than with a rounded one.

The difference in the error for the yaw moment and the error for the side force illustrates the uncertainty in the predicted center of effort for the side force. For the sharp bottom edge foil ship, the side force is predicted to act too far towards the stern. For instance, at 10 degrees drift, the error in the yaw moment is close to zero, but the side force is overestimated with approximately 10%. This indicates that the yaw moment arm is around 10% too small. For the two other geometries, the side force is predicted to act too far towards the front. For instance, for the KVLCC2 at 9 degrees drift, the error in the side force is small, while the magnitude of the yaw moment is overestimated with close to 12%, indicating that the yaw moment arm is overestimated with approximately the same amount.

6. Results

The results from the numerical experiments are presented according to each simplification in the following subsections. At the end of the result section, we also discuss the relative importance between the rudder and the hull forces and the global consequence of each simplification with route simulation models tuned based on different data.

6.1. Neglect the free surface

The effect of the free surface was tested by simulating the ship hull at different drift angles and Froude numbers, both with and without free surface modeling. The Reynolds number was kept constant to separate out potential model scale effects from the effect of the free surface alone. This was achieved by keeping a constant velocity and viscosity in the CFD simulations, while changing the acceleration of gravity to correspond to the target Froude number. As such, for each tested drift angle, there is one simulation per Froude number with VoF free surface modeling, and one double body simulation where the free surface is neglected. The simulations were done without rudder and propeller as the hull forces are believed to be most influenced by the free surface.

Non dimensional coefficients for resistance, C_D, drift-induced resistance, $C_{D,i}$, side force, C_L, and yaw moment, C_M, for drift angles 0, 6 and 9 degrees and Froude numbers 0.15, 0.2, 0.25, and 0.3 are plotted in Fig. 14. The figure also contains plots with a simplified modeling approach for the total forces shown as dashed lines. In this model, the straight-ahead resistance is taken from the simulations with the free surface present, while the drift-induced forces are added from the simulations without the free surface. Fig. 13 shows the waves generated by the ship while moving with 9 degrees drift angle, to give

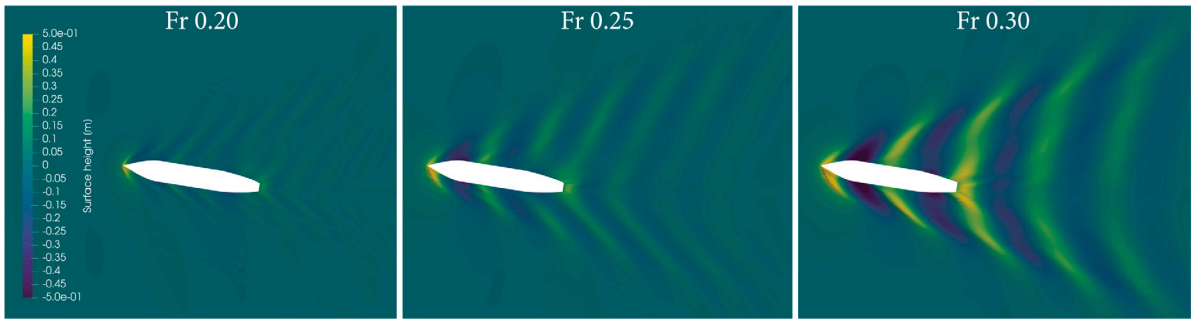

Fig. 13. Waves generated by the ship while moving with 9 degrees drift, for different Froude numbers. Model scale 1:4.

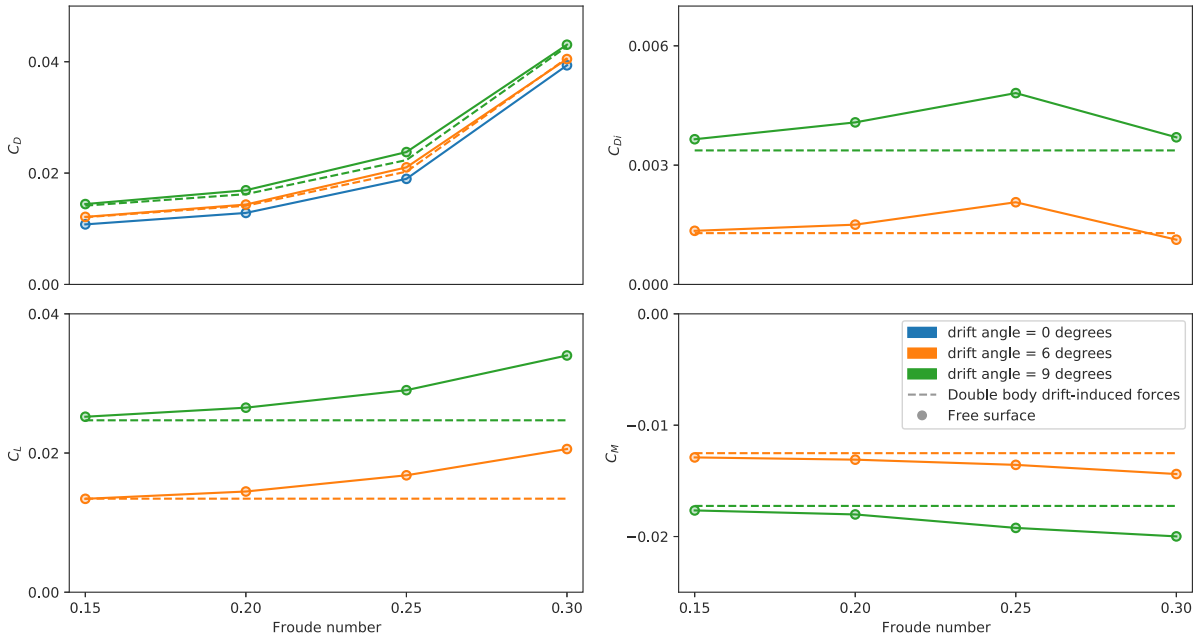

Fig. 14. Effect of Froude number on drift-induced forces. Tested at model scale 1:4 corresponding to Reynolds number of 67.8 million.

an indication of the disturbance on the free surface for the different Froude numbers.

The results show that the drift-induced forces are affected by the waves generated at the free surface, and the error is in general increasing with Froude number. This is natural as the waves generated by the ship is increasing in size with increasing Froude number as shown in Fig. 13. However, the effect is small for Froude numbers up to 0.2 and the drift-induced forces are seen to be much less affected than the straight-ahead resistance. When the Froude number is changed from 0.15 to 0.3, the straight-ahead resistance is increased with almost 300%. As a comparison, the drift-induced resistance, side force and yaw moment at 9 degrees drift is only changed by 8.9%, 27.4% and -13% respectively. We also see that the importance of the drift-induced resistance is decreasing with increasing Froude numbers. At 9 degrees, the drift-induced resistance is 33.8% of the total resistance when the Froude number is 0.15, while it is only 9.0% of the total resistance when the Froude number is 0.3. As such, if the free surface effects are only included on the straight-ahead resistance, while the drift-induced resistance is calculated with a double body simulation, the error in the total resistance is only 0.8% for Froude number 0.3 and 9 degrees drift angle.

6.2. Test in model scale

The effect of model scale was tested by simulating the ship hull at different Reynolds numbers corresponding to model scales 1:20, 1:10, 1:4, 1:2 and 1:1.33, without the free surface included in the simulation. The result is shown in Fig. 15. The resistance is shown both as the direct value from the CFD simulations and full-scale values calculated with the scaling method described in Section 3.8. The predicted full-scale straight-ahead resistance only differ by 0.56% between the actual full-scale values and those from scaled values from CFD simulations in model scale 1:20 when the friction line based on the k-ω SST model is used. This shows that the chosen scaling approach is accurate for our case study ship. For the sake of comparison, we also calculated values using the standard ITTC-57 friction line, which gave a difference of more than 7%. The drift-induced values are not scaled in any way. We observe that both the side force and the drift-induced resistance is gradually decreasing with increasing Reynolds number, while the yaw moment is less affected. The difference between full-scale and the model scale 1:20 is 51.6%, 15.5% and 3.25% for drift-induced drag, side force and yaw moment respectively, at 9 degrees drift angle. However, if the model scale is increased to 1:4, the difference from full scale is reduced to 10%, 3.7% and −0.55%. The full-scale total resistance is overpredicted by 15% when scaled values from model scale 1:20 is used, while it is overpredicted by 2.36% when the model scale 1:4 is used.

The difference in the values for the drift-induced forces are likely explained by larger cross-flow drag in model scale than in full-scale. This is natural as flow separation will happen more easily at low Reynolds numbers. An example of this is shown in Fig. 16, which show the cross-flow velocity component - i.e., the velocity in the y-direction

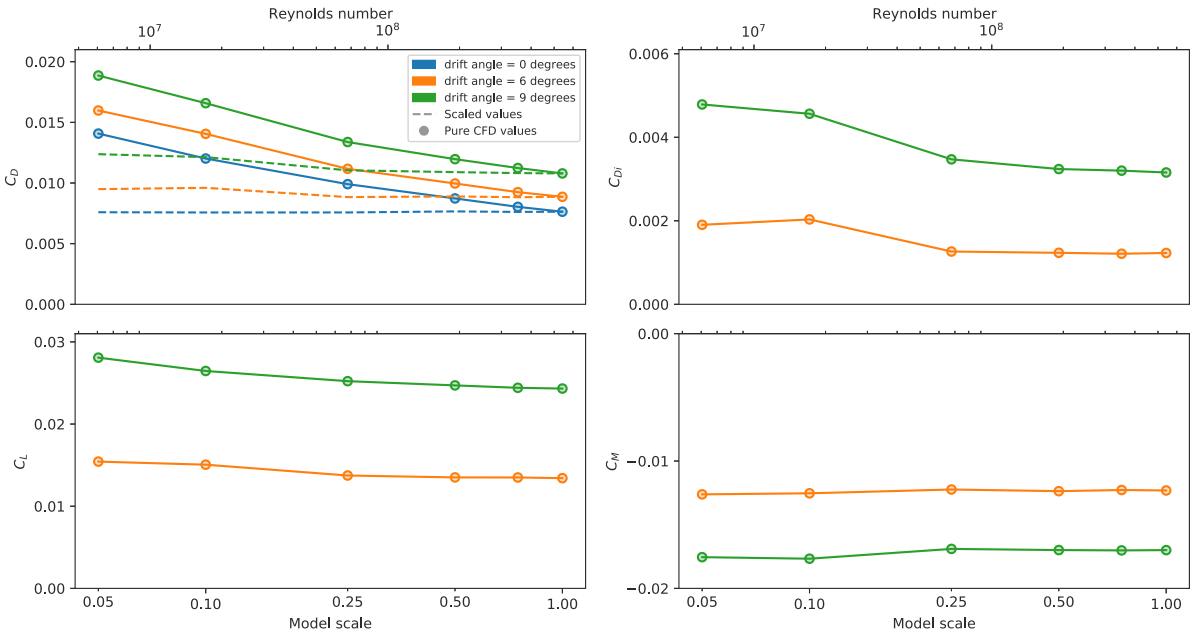

Fig. 15. Effect of model scale on the drift-induced forces.

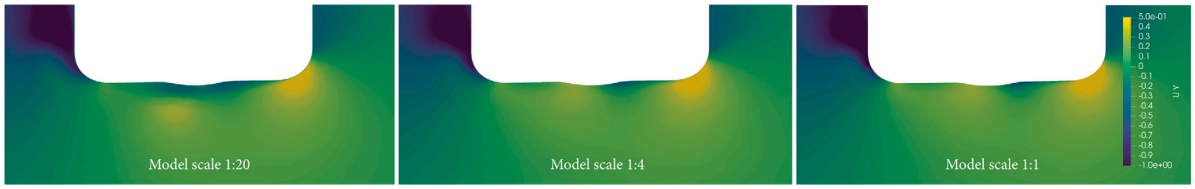

Fig. 16. Contour plot of the cross-flow velocity component at a cutting plane located 30 m from the stern, for different model scales. Both the geometry and the velocity is scaled to full-scale.

- at the same cutting plane, but different model scales. While the flow field is similar for model scale 1:4 and 1:1, there is a clear difference for model scale 1:20. The flow is clearly separating around the bottom of the ship for smallest model scale, while less so for the two other scales.

6.3. Neglect heel

The effect of heel was tested by simulating the ship hull at different heel angles and drift angles without free surface modeling in the simulation. The model scale was set to 1:4 in this test. The results can be seen in Fig. 17. The negative heel angles are in reality the most interesting tests for wind-powered cargo ships. The experienced heel angle is mostly due to the side force from the sails, which will act a large distance above the deck, in the opposite direction of the side force from the hull. This means that the ship will mostly heel to the opposite side of the hydrodynamic side force, which is the negative heel angles in the plot. The results show that the side force and resistance are not very much affected by the heel angle in the test with drift angle equal to 6 degrees. The side force at −20 degrees heel is 7% lower than the side force at 0 degrees heel, while the resistance is 2.8% higher. However, the effect of heel increases rapidly with increasing drift angle. At 9 degrees drift, the side force is reduced with almost 20% at −20 degrees heel, while the resistance is increased with 3.9%. The yaw moment is affected at both the tested drift angles. The absolute value of the yaw moment at −20 degrees heel is 45% and 48% higher than at zero degrees heel at drift angles equal to 6 and 9 degrees respectively.

The effect of heel can be modeled with simplified models based on classical linear lifting surface theory, as shown in Ross (2008). However, the fact that the effect of heel is so much larger for 9 degrees drift than 6 degrees drift suggest that non-linear cross-flow drag effects are strongly affected by the heel angle, while linear effects are less affected. As such, simplified modeling approaches are not sufficient in this case. Fig. 18 shows the cross-flow velocity component at drift angles equal to 6 and 9 degrees, and heel angles equal to 0 and -15 degrees at a cutting plane located mid-ship. The figure shows that the flow separates around the bottom edge of the ship at both drift angles when the heel angle is −15 degrees, while no separation is observed for zero heel. This illustrates that a heel angle can induce cross-flow drag on the hull-sections, which again affects the drift-induced forces and moments. If the stability of the ship is such that large heel angles are possible, they are likely to occur at the same time as large drift angles as they are the consequence of the same aerodynamic side force. Whether or not to include heel as part of the test matrix for a wind powered cargo ship design is therefore mostly a question of whether or not large heel angles are likely for the specific ship. This is dependent on the stability of the ship, and could therefore vary a great deal between different ships.

6.4. Assumption in the modified MMG model

To test the assumption in the MMG model, we used the results from CFD simulations without the free surface, at model scale 1:4, where the drift angle, rudder angle and propeller thrust coefficient is changed. There are mainly three questions we wanted to answer:

1. Is the order of the polynomial model for the hull appropriate?
2. Is the interaction model between the hull and the rudder accurate?
3. Is the interaction model between the propeller and rudder accurate?

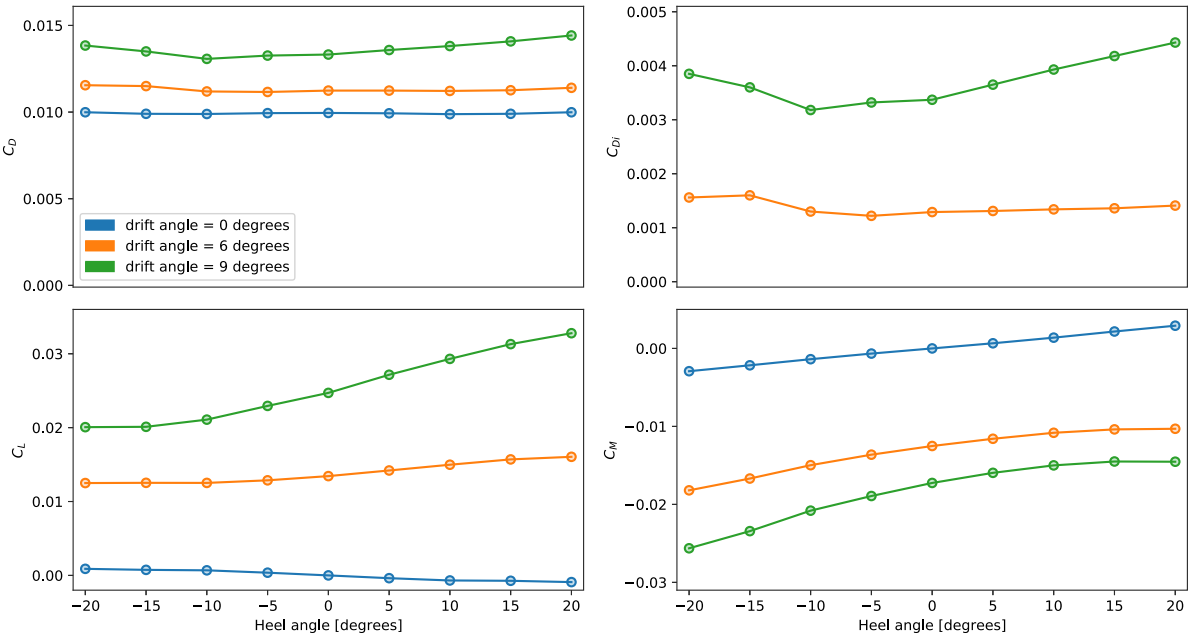

Fig. 17. Effect of heel on the drift-induced forces.

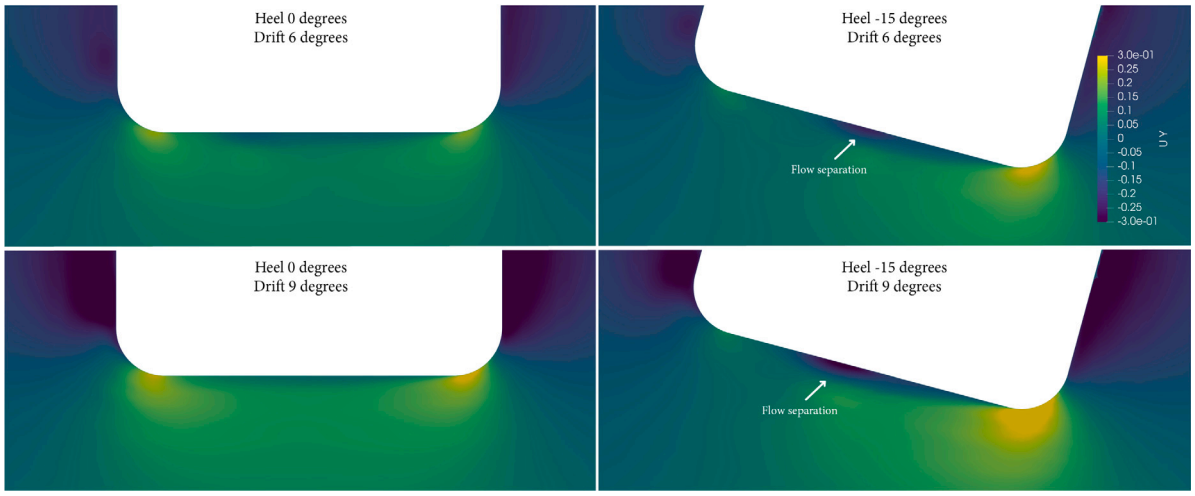

Fig. 18. Contour plot of the cross-flow velocity component for different drift and heel angles.

We explored the first question by tuning the MMG hull polynomial model using results from simulations that tested the hull alone at different drift angles. The complete data set consists of drift angles between 0 and 12 degrees, with 1 degree step size. Both the drift-induced forces and the drift-induced yaw moment are modeled using polynomials with two coefficients. The minimum number of data points necessary to tune the model is therefore two. We have plotted the results from the CFD simulations, as well as the estimated values for resistance, side force and yaw moment based on tuned model results in Fig. 19. The solid line shows the results from the polynomial hull model that is tuned based on the CFD data from drift angles 6 and 9 degrees. The lighter blue area in the figure shows the range of values between the minimum estimated value and maximum estimated value if two random data points are chosen as tuning data from the data set where the drift angle is larger than 3 degrees. This area illustrates the sensitivity of the model accuracy to the chosen tuning data. The smaller drift angles were excluded as we found this to greatly improve the results.

The rudder-induced forces on the hull are assumed to be linearly dependent on the rudder forces in the MMG model, when the body fixed coordinate system is used. In order to separate rudder-induced forces from drift induced forces, we tuned a route simulation model based on the CFD data including both the rudder and the hull. We then estimated the rudder induced forces in a CFD simulation as the direct values from the simulation minus the drift-induced values in the tuned model. The results are shown in Fig. 20 where both the CFD data and the estimated values form a tuned model is shown. Unlike most of the other plots in this paper, the body fixed coordinate system is used to show the linearity in the model. We also tried to estimate the rudder induced hull forces by comparing simulations with and without the rudder present, but this gave slightly worse results than the tuning approach. This indicates that the presence of the rudder slightly affects the drift-induced forces on the hull.

The linear model of the rudder-induced forces appears to be appropriate for both the side force and the yaw moment. The rudder induced forces along the ship's centerline does not show a clear linear

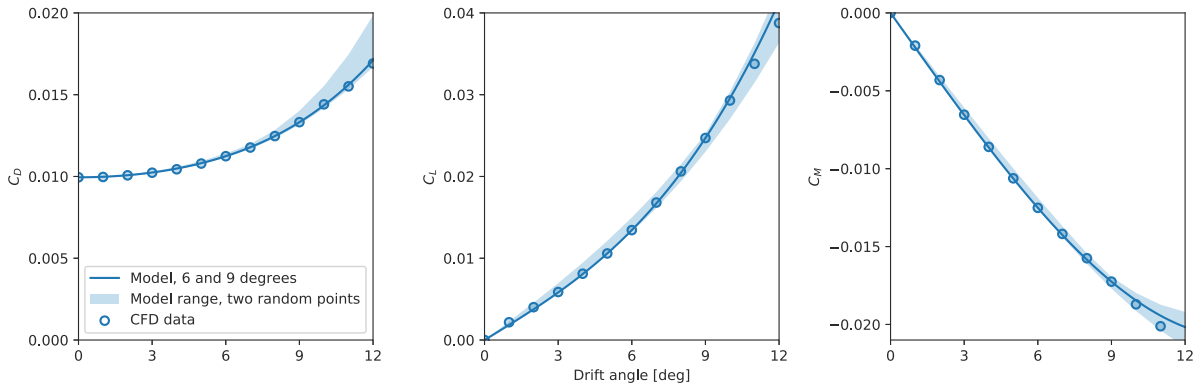

Fig. 19. Hull model in the MMG-model.

pattern, but is also seen to be very small for our case study ship. The rudder-induced hull forces in this direction are presented relative to the total hull force in the same direction in order to show the relative importance of this force. At different rudder angles, drift angles, and propeller loadings, the rudder induces a force on the hull that is around 2% of the total hull resistance at the maximum and less than 1% for most of the cases.

The final part of the verification of the MMG-based route simulation model is the rudder force model. This model was tested by comparing values directly from CFD simulations against values from tuned route simulation models. The result can be seen in Fig. 21. Both the default MMG model and our modified rudder model based on classical lifting line theory are shown. We limit the plot for the MMG model to the case with zero propeller loading in order to avoid clutter as the general trend is the same of all thrust coefficients. We also do not show plots of the yaw moment from the rudder, as both the shape and accuracy of the yaw moment is comparable to the side force plot. However, we do report the accuracy of the yaw moment model later in the text.

Only some of the data points in Fig. 21 was used to tune the models. The models for the rudder lift and drag as a function of effective rudder angle was tuned based on a static rudder test where both the drift angle and the propeller loading were zero. The total data set for the tuning procedure consisted of rudder angles equal to 0, 3, 6 and 9 degrees. The wake factor used in the model was taken as the average wake factor at the location of the rudder from a CFD simulation without the rudder present, where both the drift angle and thrust coefficient was set to zero. It is hard to separate out the effect of velocity from the effect of force coefficients in the model, and we therefore found it necessary to estimate the wake factor from the velocity field in a CFD simulation. The model for the change in rudder inflow as a function of drift angle was tuned based on a static drift test, with varying rudder angles and zero propeller loading. The included drift angles where 6, and 9 degrees, and the included rudder angle was −6 and +6 degrees. The final tuning procedure adjusts the flow acceleration factor, κ, in the propeller model. We tuned the model by minimizing the error in the predicted lift and drag from the rudder at a propeller thrust coefficient of 0.5, rudder angles of −6 and +6 degrees, and a drift angle of 6 degrees.

The average error for the lift and yaw moment is approximately 7% for both the default MMG model and our modified rudder model for cases with lift coefficient larger than 0.1. The error in the estimated drag coefficient from the standard MMG model is essentially large for all cases with an average value of 95%. The same statistics for our modified rudder model is 25%. The main issue with the modified rudder model seems to be for cases when both the thrust coefficient and drift angle is large at the same time. For cases with zero thrust coefficient or zero drift angle, the error in the drag coefficient is 10%. Including more data in the tuning procedure did not improve the results notably.

Fig. 22 shows a contour plot of the velocity over the rudder when the propeller thrust coefficient is equal to 0.5. This illustrates some of the complexity in the flow field around the rudder. The jet stream from the propeller actuator disk is clearly visible, with flow structures that vary as a function of both drift and rudder angle. The MMG model assumes that the entire effect of the propeller jet stream can be modeled with a single correction to the axial velocity. Based on the flow structures visible in Fig. 22, it does not seem strange that this simplified modeling approach is not perfect. However, the accuracy of the MMG simplification might still be acceptable for early design iterations and simplified case studies. A wind-powered ship will experience smaller thrust coefficients when the force from the sails is large. In other words, when large drift angles and rudder angles are necessary, the thrust coefficient is likely to be small. As such, the most important case for a rudder model for a wind-powered ship is the accuracy for small thrust coefficients, which was also the cases with the highest model accuracy.

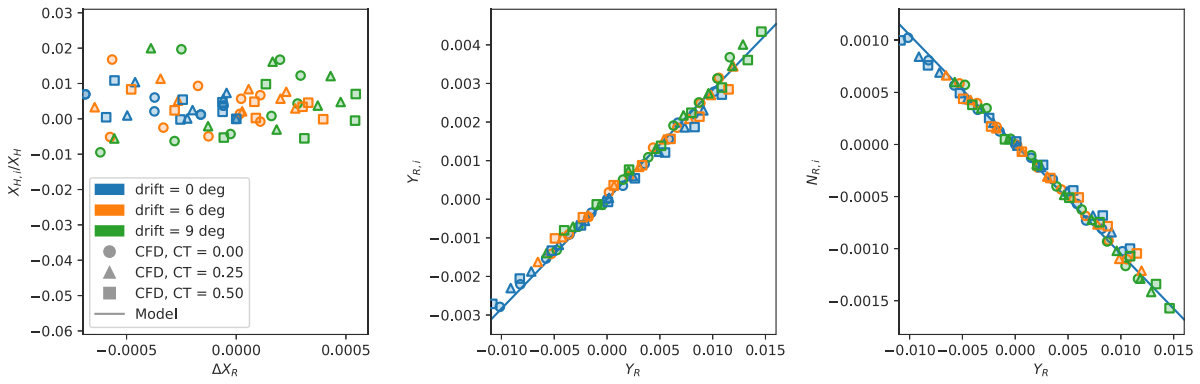

Fig. 20. Hull and rudder interaction.

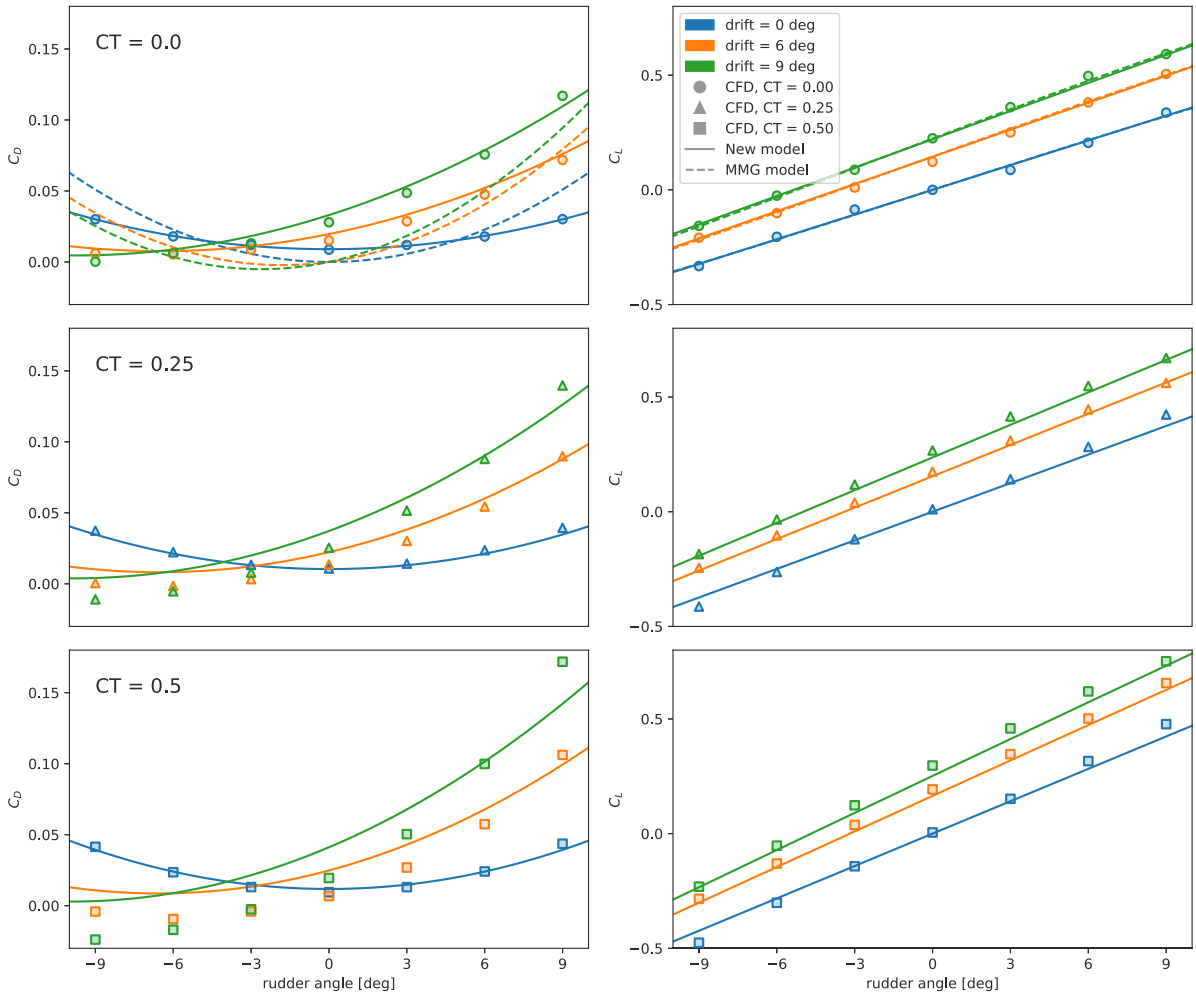

Fig. 21. Rudder forces as function of drift angle, rudder angle, and propeller loading.

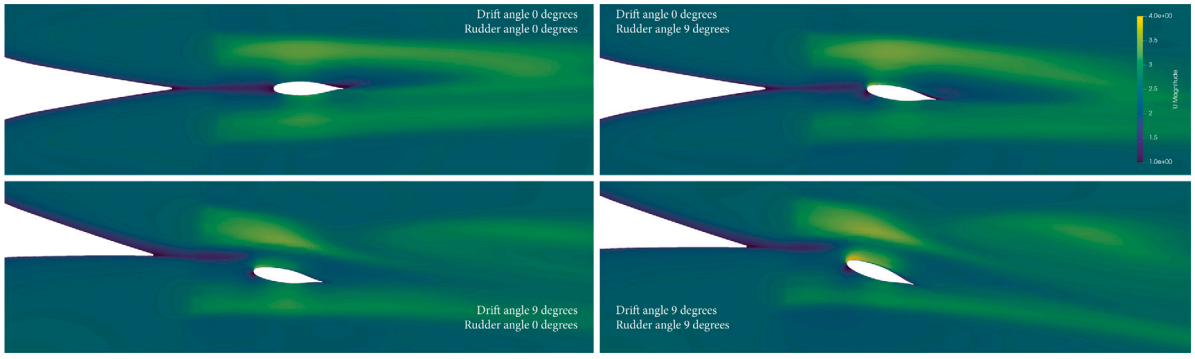

Fig. 22. Contour plot of the velocity magnitude at a cutting plane located at the same depth as the propeller center. The thrust coefficient in these simulations were 0.5.

6.5. Comparison of simulation time and global errors

The main goal of a route simulation model is to predict the resistance on the vessel at different operating conditions. The importance of the different parts of the model can therefore be evaluated by how much they contribute to the total resistance. The sources of resistance in the route simulation model can be divided into the straight-ahead resistance, drift-induced resistance, rudder resistance and rudder-induced resistance on the hull. With the exception of the straight-ahead resistance, each of the resistance components is highly dependent on the aerodynamic forces from the sail. The increase in resistance due to both drift and rudder angle is a consequence of balancing the side force and yaw moment generated from the sails. For the sake of this discussion, we have chosen to use a simplified aerodynamic model consisting of a side force vector acting at a fixed point in space where the yaw moment is dependent on the longitudinal location of the force. An overview of the simplified aerodynamic model can be seen in Fig. 23.

The amount of side force from the sails will vary depending on wind direction, sail type, and ship speed. As for instance shown in Kramer et al. (2016a), the side force produced by both a wing sail and a rotor sail can be more than 10 times as large as the thrust even at wind directions that produce significant amount of thrust. The same reference also shows that if the ship is moving two times faster than

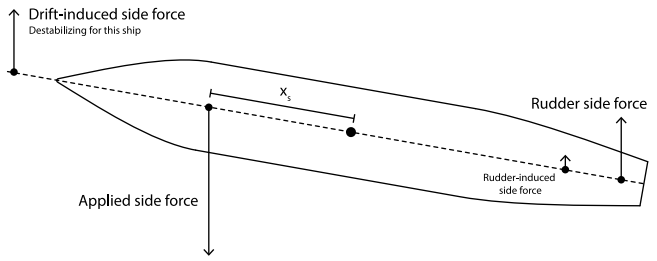

Fig. 23. Illustration of simplified aerodynamic model with resulting hydrodynamic forces.

the wind, the side force from a rotor sail can be almost 4 times as large as the thrust even at the most optimal wind direction. We have varied the side force from the sails between 0 and 3 times the straight-ahead resistance of the ship at the design speed and used the route simulation model to calculate the increase in resistance as a function of side force. The result for three different placements of the sail force vector is shown in Fig. 24. The model is tuned based on the CFD data for model scale 1:4 and the assumed thrust coefficient in the model is 0.25. The figure shows that the source of the increase in resistance varies depending on the placement of the side force. When the side force are placed towards the bow of the ship, the drift-induced resistance on the hull is the largest part of the added resistance. The rudder becomes more and more important as the placement of the side force is shifted backwards.

Both the rudder and the drift-induced resistance is a large part of the increase in resistance and both therefore deserve accurate modeling. Somewhat surprisingly, the increase in resistance due to the side force is fairly constant for different sail placements for our case study ship. The sail-induced increase in resistance on the ship is around 6%, 18% and 35% for side force ratios of 1, 2 and 3. We consider both the main dimensions and the rudder aspect ratio and size to be fairly typical for this type of ships. The fact that the low-aspect ratio hull is capable of balancing the side force approximately as efficiently as the rudder is therefore interesting. The explanation is likely that the hull is producing the lift with a very low loading relative to the representative area. As lift-induced drag is typically assumed to be proportional to the lift coefficient squared, it seems reasonable that the resistance increase is small, even with the low aspect-ratio. The drift and rudder angles experienced by the ship also varies depending on the placement of the sails. The drift angle is less than 8 degrees for all the test cases in the figure, while rudder angle is as large as 16 degrees for the sail placement at the middle of the ship. We also tested sail-placements further towards the stern, but this quickly resulted in rudder angles approaching a likely stall limit. This indicates that the rudder is probably too small for balancing large sails placed towards the stern, and that the placement of the sails should either be towards the front, or the size of the rudder should increase.

To evaluate the global consequence of each simplification, we tuned the route simulation model based on different CFD simulations and computed the resistance as a function of side force. The left plot shown in Fig. 25 show the consequence of different simplifications for the drift induced hull forces. The route simulation model is balanced using only the drift angle. Although this is technically not possible for our case study ship, since some amount of rudder force is necessary to achieve yaw moment balance, the purpose is to show the worst possible consequence of each simplification for the drift-induced forces. We then did the same exercise, with the rudder included, and both rudder models. The result is shown in the right plot in Fig. 25. Both the yaw moment and the side force are balanced. The drift induced forces are simulated at a model scale of 1:4, without the free surface resent, and the thrust coefficient is assumed to be 0.25. We also tested the ship with CFD with the same values for the drift and rudder angle as the tuned model for side force ratios of 1, 2 and 3.

When the side force ratio is 3, the double body model underestimates the resistance with 1.4% relative to the CFD simulations with free surface modeling. The difference between model scale 1:10 and model scale 1:4 is 5.2%. The difference between the model tuned from the data with 10 degrees heel and the same data at zero degrees heel is 9.6%. The difference between the standard MMG rudder model and our modified rudder model is 39% for the largest side force ratio. We also see that our new model fits well with the data directly from the CFD simulations.

These errors must be evaluated against simulation time. We measured the clock-time for each simulation in this paper, executed on the same computer. Neglecting the free surface reduced the simulation time from almost 8 h to just above 1, when the model scale was 1:4. This is therefore a simplification with a large reduction in simulation time, but with just a small error in the resistance model. A full-scale simulation without the rudder took around 2.3 h, compared to around 0.8 h in model scale 1:10. This shows that model scale 1:4 is comparable to model scale 1:10 in simulation time, while the simulation results is comparable to full-scale values. Neglecting heel mainly has the consequence that we can run fewer simulations. As such, including heel in the test matrix will increase the total simulation time with a factor of 2–3 depending on the number of heel angles one decides to test. However, the error in the added resistance can be quite large, and this might be necessary for ships where the stability is not sufficient to avoid larger heel angles.

7. Conclusion

Although there was a clear effect of the free surface on the drift induced forces for our case study ship, the effect was much smaller than on the straight-ahead resistance. The importance of the drift-induced forces is also reduced for increasing Froude number, as the importance of the wave resistance is increasing. Considering the large decrease in computational time achieved by neglecting the free surface, this is a simplification that is worth considering for design studies of wind powered cargo ships. For Froude numbers around 0.2 or less, the free surface seems to be safely neglected, both based on the experiments done in this paper and the other references from the literature. Slightly higher Froude numbers could also be considered, although the error due to this simplification was shown to increase along with the Froude number.

We found that the error due to too low Reynolds number is fairly large for model scales in the range typically used in towing tanks, shown both in our experiments and in other papers in the literature. The explanation is likely that the flow around the bottom of the hull separates more easily at lower Reynolds numbers, which leads to larger cross-flow drag. However, the error is reduced to a minimum for model scales larger than 1:4 for our case study ship. This represents a Reynolds number of 67.7 million and model length of 30 m. Although this would be a very large model for a towing tank experiment, it is still small enough to be a time efficient scale for CFD simulations. As such, it seems that drift-induced forces can accurately be predicted at practical model scales for CFD simulations, but scales typical for towing tanks should be avoided if possible.

The effect of heel turned out to be large when large heel angles were combined with large drift angles. This is expected to be due to changes in the cross-flow drag on the ship as a function of heel. Whether or not heel should be part of the test program for a wind-powered ship is therefore primarily a question about ship stability. If the expected heel angles due to wind power approaches 10 or 15 degrees, a more comprehensive test program and route simulation model are probably necessary.

The hull forces due to both drift and rudder angle was predicted well with the polynomials in the MMG model. The default rudder model was, however, not very accurate for computing the rudder resistance. This was not surprising considering the simplicity of the model. The

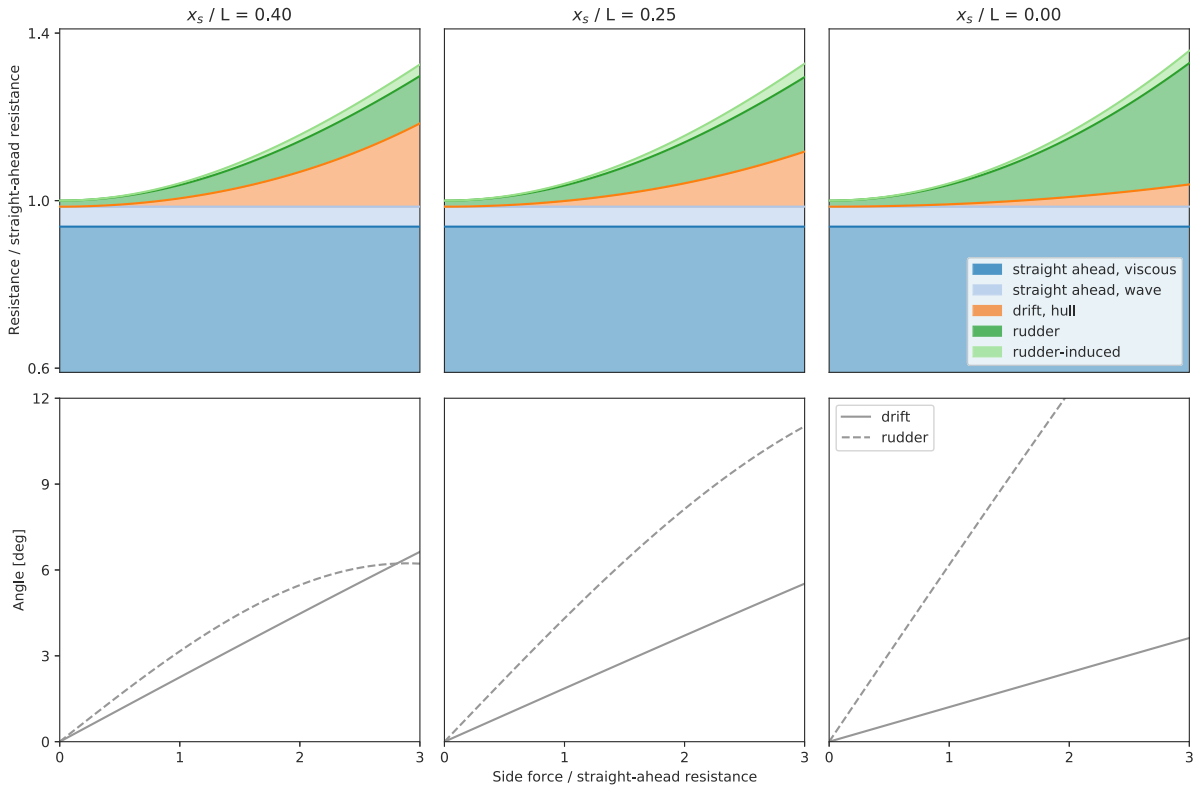

Fig. 24. Importance of different resistance components.

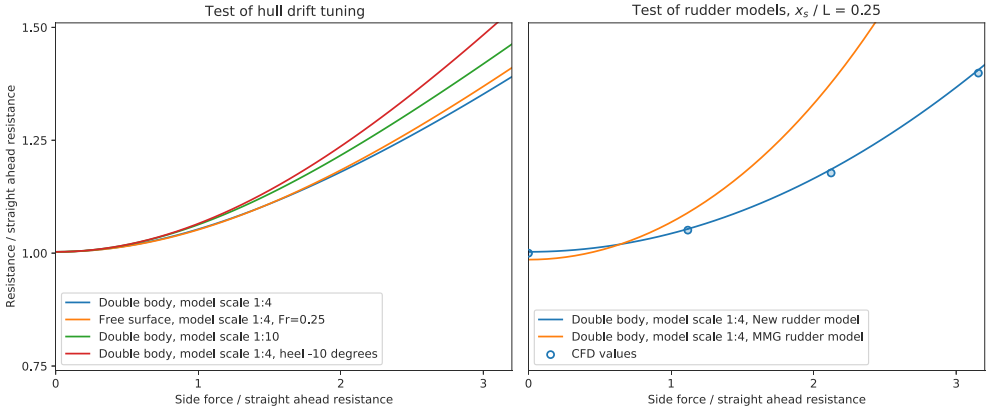

Fig. 25. Comparison of models.

accuracy was greatly improved by switching to a more conventional model for lifting surfaces based on classical lifting line theory. With the new model, the rudder forces could be estimated accurately as a function of drift angle and rudder angle using just a few CFD simulations as tuning data. Although it was not perfect, the main problem with the model was predicting the forces when both the drift angle was large, and the propeller thrust coefficient was high at the same time. This is expected to be due to a complex flow field in the jet from the propeller, that are affected by both propeller thrust, drift angle and rudder angle at the same time. However, the purpose of a sail is to reduce the required thrust from the propeller and the main problem with the model will therefore reduce as the amount of thrust from the sails increase. Although it is likely possible to find more advanced models that better capture the dynamics between the rudder and the propeller, this would probably entail more variables that needs to be tuned based on either CFD or experimental data. We therefore conclude that the modified MMG model is a good compromise for quick design iterations and simplified case studies.

As an interesting note, the rudder resistance was found to be as large or larger than the drift-induced hull resistance for our case study ship, depending on the placement of the sails. This was somewhat surprising, and indicate that both sources of resistance deserve equal amount of attention during a design loop.

CRediT authorship contribution statement

Jarle Vinje Kramer: Conceptualization of this study, Methodology, Software, Writing. **Sverre Steen:** Assistance in conceptualization of this study, Guidance, Text revision.

Declaration of competing interest

The authors declare that they have no known competing financial interests or personal relationships that could have appeared to influence the work reported in this paper.

Acknowledgment

This work was carried out at SFI Smart Maritime (WP2) supported by the Research Council of Norway through the Center for Research-based Innovation (SFI) scheme (Grant number 237917).

References

Abkowitz, M.A., 1964. Lectures on Ship Hydrodynamics Steering and Manoeuvrability. Technical Report, Technical Univeristy of Denmark, Lyngby, Denmark.

Bertram, V., 2000. Practical Ship Hydrodynamics. Butterworth Heinemann.

Bhushan, S., Xing, T., Carrica, P., Stern, F., 2009. Model- and full-scale URANS simulations of athena resistance, powering, seakeeping, and 5415 maneuvering. J. Ship Res. 54 (4), 179–198.

DNV-GL, 2016. Rules For Classification, Part 3 Hull, Chapter 15 Stability. Technical Report, DNV-GL.

Duman, S., Bal, S., 2019. A quick-responding technique for parameters of turning maneuver. Ocean Eng. 179, 189–201.

Eça, L., Hoekstra, M., 2008. The numerical friction line. J. Mar. Sci. Technol. 13, 328–345.

Eça, L., Hoekstra, M., 2014. A procedure for the estimation of the numerical uncertainty of CFD calculations based on grid refinement studies. J. Comput. Phys. 262, 104–130.

Eça, L., Vaz, G., Hoekstra, M., 2010. Code verification, solution verification and validation in RANS solvers.

Goldstein, S., 1929. On the vortex theory of screw propellers. Proc. R. Soc. A 123 (792), 440–465.

Hirt, C.W., Nichols, B.D., 1981. Volume of fluid (VOF) method for the dynamics of free boundaries. J. Comput. Phys. 39 (1), 201–225. http://dx.doi.org/10.1016/0021-9991(81)90145-5.

Hympendahl, O., Ciortan, C., 2018. Systematic assessment of model errors in CFD ship resistance simulations. In: Proceedings of Numerical Towing Tank Symposium. Cortona Italy.

International Towing Tank Conference, 2011. Practical Guidlines for Ship CFD Applications. Technical Report, International Towing Tank Conference.

International Towing Tank Conference, 2017. Uncertainty Analysis in CFD Verification and Validation Methodology and Procedures. Technical Report, International Towing Tank Conference.

Issa, R.I., Gosman, A.D., Watkins, A.P., 1986. The computation of compressible and incompressible recirculating flows by a non-iterative implicit scheme. J. Comput. Phys. 62 (1), 66–82. http://dx.doi.org/10.1016/0021-9991(86)90100-2.

Jin, Y., Duffy, J., Chai, S., Chin, C., Bose, N., 2016. URANS study of scale effects on hydrodynamic manoeuvringcoefficients of KVLCC2. Ocean Eng. 118, 93–106.

van der Kolk, N.J.V.D., Akkerman, I., Keuning, J.A., Huijsmans, R.H.M., 2020. Part 2: Simulation methodology and numerical uncertainty for RANS-CFD for the hydrodynamics of wind-assisted ships operating at leeway angles. Ocean Eng. 201.

van der Kolk, N.J.V., Keuning, J.A., Huijsmans, R.H.M., 2019. Part 1: Experimental validation of a RANS-CFD methodology for the hydrodynamics of wind-assisted ships operating at leeway angles. Ocean Eng. 178, 375–387.

Kramer, J.V., 2021. GitHub page for the article "Simplified test program for hydrodynamic CFD simulations of wind-powered cargo ships". https://github.com/jarlekramer/Hydrodynamic-test-program-for-wind-power.

Kramer, J., Steen, S., 2015. Importance of the free surface for the drift-induced forces on a ship-like foil. In: Numerical Towing Tank Symposium. Cortona, Italy.

Kramer, J., Steen, Savio, L.S., 2016a. Drift forces–wingsails vs flettner rotors. In: High-Performance Marine Vehicles. Cortona.

Kramer, J., Steen, S., Savio, L., 2016b. Experimental study of the effect of drift angle on a ship-like foil with varying aspect ratio and bottom edge shape. Ocean Eng. 121, 530–545.

Kume, K., Hasegawa, J., Tsukada, Y., Fujisawa, J., Fukasawa, R., Hinatsu, M., 2006. Measurements of hydrodynamic forces, surface pressure, and wake for obliquely towed tanker model and uncertainty analysis for CFD validation. J. Mar. Sci. Technol. 11, 65–75.

Larsson, L., Stern, F., 2014. Numerical Ship Hydrodynamics - An Assessment of the Gothenburg 2010 Workshop. Springer.

Longo, J., Stern, F., 2002. Effects of drift angle on model ship flow. Exp. Fluids 32 (5), 558–596.

Menter, F.R., Kuntz, M., Langtry, R., 2003. Ten years of industrial experience with the SST turbulence mode. In: Proceedings of the Fourth International Symposium on Turbulence, Heat and Mass Transfer. Antalya, Turkey.

Molland, A.F., Turnock, S.R., 1995. Wind Tunnel Tests on the Effect of a Ship Hull on Rudder-Propeller Performance at Different Angles of Drift. Technical Report, University of Southampton, Southampton, England.

Molland, A.F., Turnock, S.R., 2002. Flow straithtening effects in a ship rudder due to upstream propeller and hull. Int. Shipbuild. Prog. 49, 195–214.

Ohashi, K., Kobayashi, H., Hino, T., 2018. Numerical simulation of the free-running of a ship using the propeller model and dynamic overset grid method. Ship Technol. Res. 65, 153–162.

Oosterveld, M.W.C., Oossanen, P.V., 1975. Further computer-analyzed data of the wageningen B-screw series. Int. Shipbuild. Prog. 22.

OpenCFD ltd, 2021. OpenFOAM homepage. https://www.openfoam.com/.

Ouchi, K., Uzawa, K., Kanai, A., Katori, M., 2013. "Wind Challenger" the next generation hybrid sailing vessel. In: Proceedings of the Third International Symposium on Marine Propulsors.

Patankar, S.V., Spalding, D.B., 1983. A calculation procedure for heat, mass and momentum transfer in three-dimensional parabolic flows. Int. J. Heat Mass Transfer 15 (10), 1787–1806. http://dx.doi.org/10.1016/0017-9310(72)90054-3.

Perić, R., Abdel-Maksoud, M., 2016. Reliable damping of free-surface waves in numerical simulations. Ship Technol. Res. 63, 1–13.

Raven, H.C., van der Ploeg, A., Starke, A.R., Eca, L., 2008. Towards a CFD-based prediction of ship performance—progress in predicting full-scale resistance and scale effects. Int. J. Marit. Eng. 150.

Richardson, L.F., 1911. The approximate arithmetical solution by finite differences of physical problems involving differential equations, with an application to the stresses in a masonry dam. Phil. Trans. R. Soc. A 210 (459-470), 307–357.

Ross, A., 2008. Nonlinear Manoeuvring Models for Ships: A Lagrangian Approach. Technical Report, Norwegian University of Science and Technology, Trondheim, Norway.

Spalart, P.R., Rumsey, C.L., 2007. Effective inflow conditions for turbulence models in aerodynamic calculations. AIAA J. 45, 2544–2553.

Tillig, F., 2020. Simulation Model of a Ship's Energy Performance and Transportation Costs. Technical Report, Chalmers Univeristy of Technology, Gothenburg, Sweden.

Tillig, F., Ringsberg, J.W., 2020. Design, operation and analysis of wind-assisted cargo ships. Ocean Eng. 211.

Tillig, F., Ringsberg, J.W., Psaraftis, H.N., Zis, T., 2020. Reduced environmental impact of marine transport through speed reduction and wind assisted propulsion. Transp. Res. D 83.

Väinämö, J., 2017. Operational experience and results from the first reference installation from Nov-2014, roro-ship estraden (9700 DWT). In: 24th International HISWA Symposium on Yacht Design and Yacht Construction. Amsterdam, Netherlands.

Virtanen, P., Gommers, R., Oliphant, T.E., Haberland, M., Reddy, T., Cournapeau, D., Burovski, E., Peterson, P., Weckesser, W., Bright, J., van der Walt, S.J., Brett, M., Wilson, J., Millman, K.J., Mayorov, N., Nelson, A.R.J., Jones, E., Kern, R., Larson, E., Carey, C.J., Polat, I., Feng, Y., Moore, E.W., VanderPlas, J., Laxalde, D., Perktold, J., Cimrman, R., Henriksen, I., Quintero, E.A., Harris, C.R., Archibald, A.M., Ribeiro, A.H., Pedregosa, F., van Mulbregt, P., SciPy 1.0 Contributors, 2020. SciPy 1.0: Fundamental algorithms for scientific computing in python. Nature Methods 17, 261–272. http://dx.doi.org/10.1038/s41592-019-0686-2, URL: https://rdcu.be/b08Wh.

Yasukawa, H., Yoshimura, Y., 2015. Introduction of MMG standard method for ship maneuvering predictions. J. Mar. Sci. Technol. 20, 37–52.